Modeling of Third-order Distortion in Common-Emitter SiGe HBTs Using Mextram 505.00

by

Xuewei Ding

A thesis submitted to the Graduate Faculty of
Auburn University
in partial fulfillment of the
requirements for the Degree of
Master of Science

Auburn, Alabama
April 5, 2018

Keywords: Mextram SiGe HBT, Capacitance, IP3, ICCAP

Approved by

Guofu Niu, Professor of Electrical and Computer Engineering
Fa Foster Dai, Professor of Electrical and Computer Engineering
Bogdan Wilamowski, Professor of Electrical and Computer Engineering

Abstract

Mextram is an advanced compact model for bipolar transistors. Mextram 504.12 does not provide a good OIP3 simulation near peak OIP3. Mextram 505.00 improves peak OIP3 by modifying intrinsic base-collector depletion capacitance. As for the intrinsic CB depletion capacitance, Mextram 505.00 modifies control voltage V_{junc} and smooth transition width V_{ch} to help OIP3 simulation. At the same time, Mextram 505.00 provides several options for V_{junc} and V_{ch}.

In Mextram 504.12, V_{junc} is the main reason for distorted peak OIP3. V_{junc} goes up quickly once high injection occurs, as the zero injection epilayer resistance is used to calculate V_{junc} as $V_{B_2C_1} + V_{xio}$, with V_{xio} being $x_i = 0$ resistance calculated epilayer voltage drop. This V_{junc} needs a very large V_{ch} to smooth the control voltage so that the intrinsic CB depletion capacitance increases gradually, but this V_{ch} also distorts both the intrinsic CB depletion capacitance and peak OIP3. Mextram 505.00 fixes V_{junc} and V_{ch} to provide a much better OIP3 simulation.

To investigate how the intrinsic CB depletion capacitance affects OIP3. Contributions to the third order output current are individually examined. The third order main current is found to be dominant, and sensitive to V_{junc} and V_{ch}. The intrinsic CB depletion capacitance affects the third order main current through circuit action. The extrinsic CB depletion capacitance also has a big effect on OIP3 through the third order main current. Decreasing the extrinsic CB depletion capacitance improves the peak OIP3.

Acknowledgments

I would like to express my deepest appreciation to my advisor Dr. Guofu Niu for his full support, expert guidance and encouragement throughout my study. Without his guidance and persistent help this dissertation would not have been possible. In addition, I express my gratitude to Dr. Dai and Dr. Wilamowski for their thoughtful comments and precious time.

I would like to thank Dr. Andries Scholten and Marnix Willemsen for measurement data.

I am very much thankful to my group mates for their support and encouragement.

Finally, I would like to acknowledge with gratitude, the support and love of my family. They are the power that help me work through everything.

Table of Contents

List of Figures

List of Tables

Chapter 1

Introduction

1.1 SiGe HBT Fundamentals

The Silicon-Germanium heterojunction bipolar transistor (SiGe HBT) has gained world-wide attention, and it is a type of bipolar junction transistor (BJT) which uses differing semiconductor materials for the emitter and base regions, creating a heterojunction. The HBT improves the BJT in that it can get higher current gain, higher cut-off frequency and lower base resistance compared with Si BJT. The heart of SiGe technology is band gap engineering. Adding Ge to Si BJT introduced a number of exciting performance improvements.

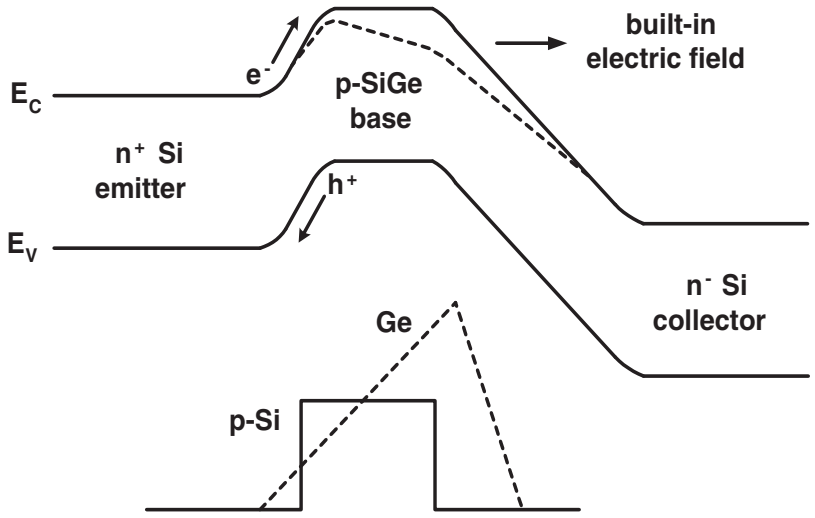

Figure 1.1: Energy band diagrams of a graded-base SiGe HBT and a Si BJT. [1]

The base region of SiGe HBTs is typically the region where SiGe alloy is used instead of Si. The basic operational principle of SiGe HBT is the band diagram shown in Figure 1.1. It illustrates the different energy-band diagrams between SiGe HBT and Si BJT by showing both biased identically in forward-active mode. The Ge profile linearly increases from zero

near emitter-base (EB) junction to some maximum value near collector-base (CB) junction, and then rapidly ramps down to zero [2]. Since the energy band gap of Ge is smaller than that of Si, adding germanium into the base region of the transistor leads to an additional band gap shrinkage, which is approximately 75 meV for each 10 percent of Ge introduced[3]. The reduction of band gap decreases transit time, which gives a higher f_T, and it also increases electron injection, which leads to a higher β. At the same collector current density, compared with normal BJT, SiGe HBT has a higher base doping, which reduces base resistance.

1.2 Mextram Basics

Mextram is an advanced compact model for bipolar transistors. Mextram has proven excellent for Si and SiGe processes, including analog, mixed-signal, high speed RF as well as high voltage high power technologies. It has an epi-layer model for high injection, and also accounts for self heating, avalanche, low-frequency and high frequency noises in physical manners. Mextram is formulated with minimal interactions between DC and AC characteristics that simplifies parameter extraction [4]. Development of Mextram was never stopped following the requirements of updated technologies. The latest version is Mextram 505.00.

In Mextram 505.00, there are 7 internal nodes and 121 parameters. Some parts of the model are optional and can be switched on or off by setting model flag parameters including the extended modeling of reverse behavior, the distributed high-frequency effects, and the increase of the avalanche current, when the current density in the epilayer exceeds the doping level.

Figure 1.2 shows the full equivalent circuit of Mextram model as it is specified in its latest release 505.00 [4]. C, B, E and substrate S are extrinsic terminals. B_2, C_2, and E_1 are intrinsic NPN terminals. B_1 is an internal node for base resistance related parasitic effects. C_1, C_3 and C_4 are internal nodes for collector resistance related parasitic effects, the most significant of which is the epilayer related quasi-saturation effect. C_3 and C_4 are for distributive buried layer resistance effects and turned off by default. I_N, I_{B_1}, I_{B_2}, I_{avl}, Q_{BE},

Q_{BC}, Q_{tE}, Q_{tC}, Q_E are placed between C_2, B_2 and E_1 to model the intrinsic NPN transistor. I_N is the main electron transport current, I_{B_1} and I_{B_2} are forward ideal and non-ideal base currents, I_{avl} is avalanche current. Q_{tE} and Q_{tC} are EB and CB junction depletion charges. Reverse base currents are modeled by the parasitic PNP base currents I_{ex} and I_{B_3}, and PNP emitter to collector transport current I_{sub} [4].

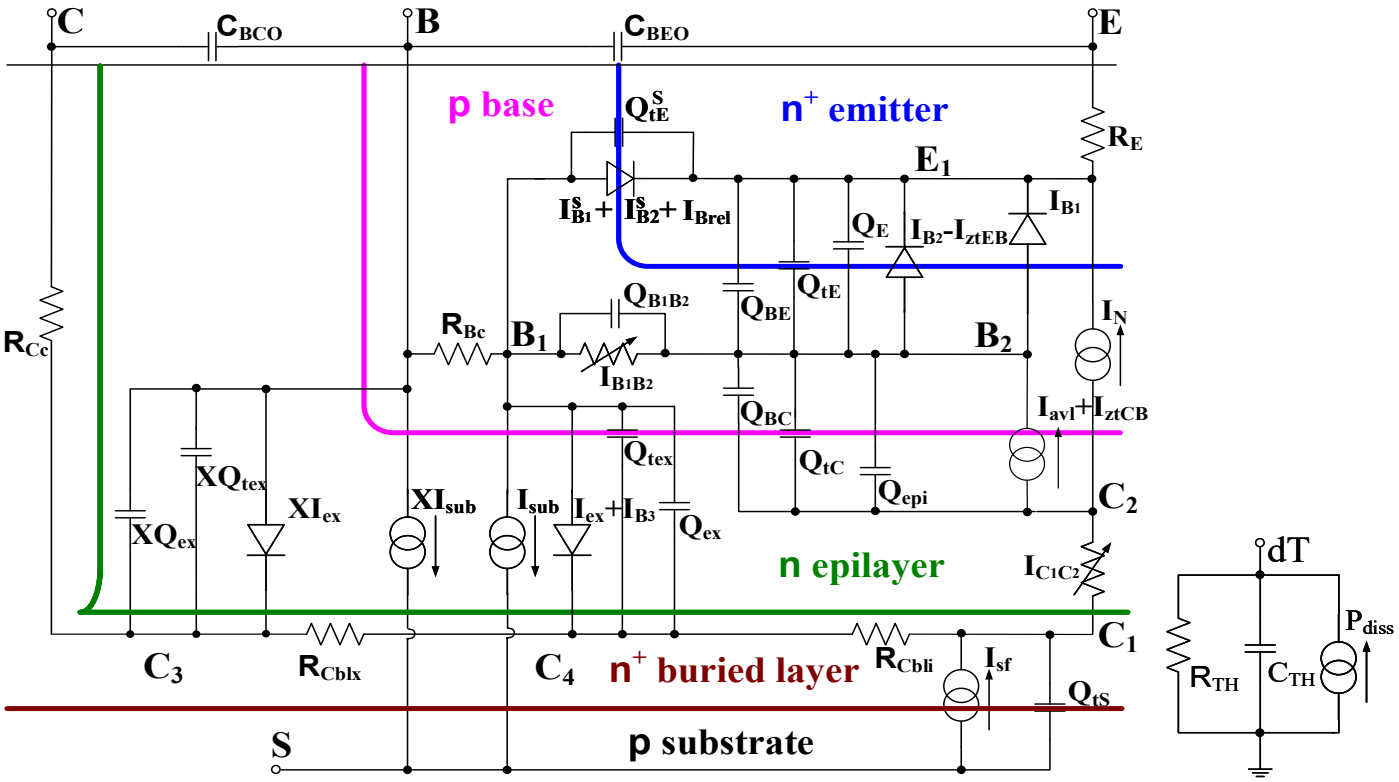

Figure 1.2: The full Mextram equivalent circuit for the vertical NPN transistor. [4]

1.3 Distortion/Linearity

When the input signal is sufficiently weak, the operation of a transistor circuit is linear and dynamic. For larger input signals, an active transistor circuit becomes a nonlinear dynamic system. Many of the nonlinear concepts, however, can be illustrated using simple power series.

Under small-signal input, the output voltage $y(t)$ of a circuit can be related to its input voltage $x(t)$ by a power series

$$y(t) = k_1 x(t) + k_2 x^2(t) + k_3 x^3(t), \tag{1.1}$$

where for simplicity we have truncated the series at third-order. The linear concepts of "harmonics" and "gain compression" are introduced below using Eq. (1.1)

1.3.1 Harmonics

If the input voltage is $x(t) = A\cos\omega t$, the output voltage $y(t)$ then becomes

$$\begin{aligned} y(t) &= k_1 A\cos\omega t + k_2 A^2\cos^2\omega t + k_3 A^3\cos^3\omega t \\ &= \frac{k_2 A^2}{2} && \text{dc shift} \\ &+ (k_1 A + \frac{3k_3 A^3}{4})\cos\omega t && \text{fundamental} \\ &+ \frac{k_2 A^2}{2}\cos 2\omega t && \text{second harmonic} \\ &+ \frac{k_3 A^3}{4}\cos 3\omega t && \text{third harmonic} \end{aligned} \quad . \tag{1.2}$$

Eq. (1.2) has a dc shift, a "fundamental output" at ω, a "second-order harmonic term" at 2ω, and a "third-order harmonic term" at 3ω. Thus, an "nth-order harmonic term "is proportional to A^n. In practice, the relative level of a given harmonic with respect to the fundamental output is of great interest.

1.3.2 Gain Compression and Expansion

The small-signal gain is obtained by neglecting the harmonics. In Eq. (1.2), the small-signal gain is k_1 when the nonlinearity-induced term $3k_3A^3/4$ is neglected. However, as the signal amplitude A grows, $3k_3A^3/4$ becomes comparable to or even larger than k_1A. The gain

thus changes with the input. This variation of gain with input signal level is a fundamental manifestation of nonlinearity [3].

If $k_3 < 0$, then $3k_3A^3/4 < 0$. That is, the gain decreases with increasing input level (A), and eventually diminishes to zero. This phenomenon is referred to as "gain compression"in many RF circuits, and is often quantified by the "1dB compression point,"or P_{1dB}. In real circuits, three terms of the power series are not usually sufficient to describe the nonlinear behavior at the 1dB compression point, because of large-signal operation. Once again, either the input or the output value can be used for characterization purposes. The input value is the input magnitude at which the gain drops by 1dB. Signal power as opposed to voltage is often used in RF circuits. The transformation between voltage and power involves a reference impedance, usually 50Ω. Typical RF front-end amplifiers require -20dBm to -25dBm input power at the 1dB compression point [3].

1.3.3 IP3

A diagram that can tie both kinds of nonlinearity discussed above is shown in Figure 1.3. For small but increasing input signal with amplitude A, the fundamental output grows linearly with it, whereas the 3^{rd} order output term increases cubically. Plotted on a decibel power scale, the fundamental grows with a 1:1 slope with input signal power, and the 3^{rd} order output grows with a 3:1 slope [5].

P_{1dB} is the point where the fundamental output stops growing with a 1:1 relationship between output and input, and gain compression sets in. The hypothetical extensions and intersection of the fundamental output curve and the 3^{rd} output curve gives us what is called the 3^{rd} order Intercept Point (IP3), and is the benchmark by which amplifier linearity is quantified. The X-coordinate of IP3 is known as the Input Third-Order Intercept Point (IIP3), and the Y-coordinate of IP3 is known as the Output Third-Order Intercept Point (OIP3). IIP3 and OIP3 are very key figures of merit, and will be used extensively in later chapter to quantify linearity [5].

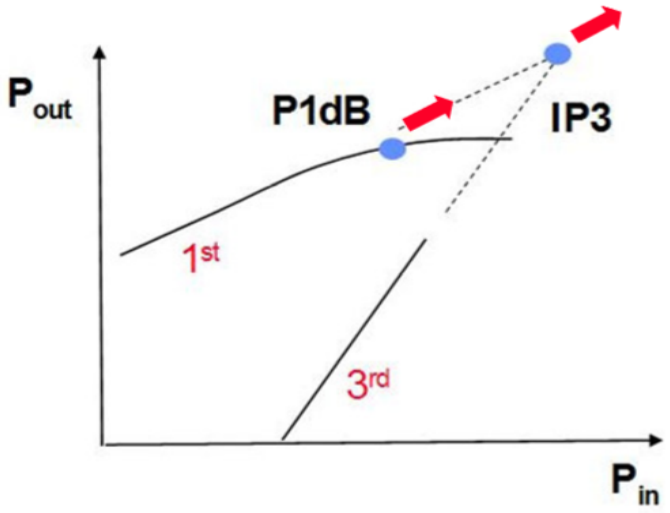

Figure 1.3: Fundamental 1^{st} and 3^{rd} order output power P_{out} versus input signal power P_{in} [5].

1.4 OIP3 simulation using Mextram 504.12 and 505.00

Figure 1.4 (a) (b) show measured and simulated harmonic OIP3 in common emitter configuration. In this OIP3 measurement and simulation process, the first order measurement and simulation are at 2GHz and the third order measurement and simulation are at 6GHz. Figure 1.4 (a) shows that measured OIP3 in dBm versus V_{BE} together with simulated OIP3 using Mextram 504.12 when $V_{CE} = 1.5V$ is fixed. Figure 1.4 (b) shows measured and simulated OIP3 in the same situation, but OIP3 is simulated using Mextram 505.00. In these two figures the blue line is OIP3 simulation and the red symbol is OIP3 measurement. OIP3 simulation using Mextram 504.12 has a big distortion near peak OIP3 compared to the measurement. Parameters that are used in Mextram 504.12 OIP3 simulation are extracted from DC and AC measurement and simulation depending on Parameter Extraction for Bipolar Transistor Model Mextram. That is to say the OIP3 distortion is not from parameter extraction and the distortion in OIP3 cannot be solved by parameter extraction. OIP3 simulated using Mextram 505.00 is really close to the measurement and it is much better than OIP3 simulated using Mextram 504.12 near peak OIP3.

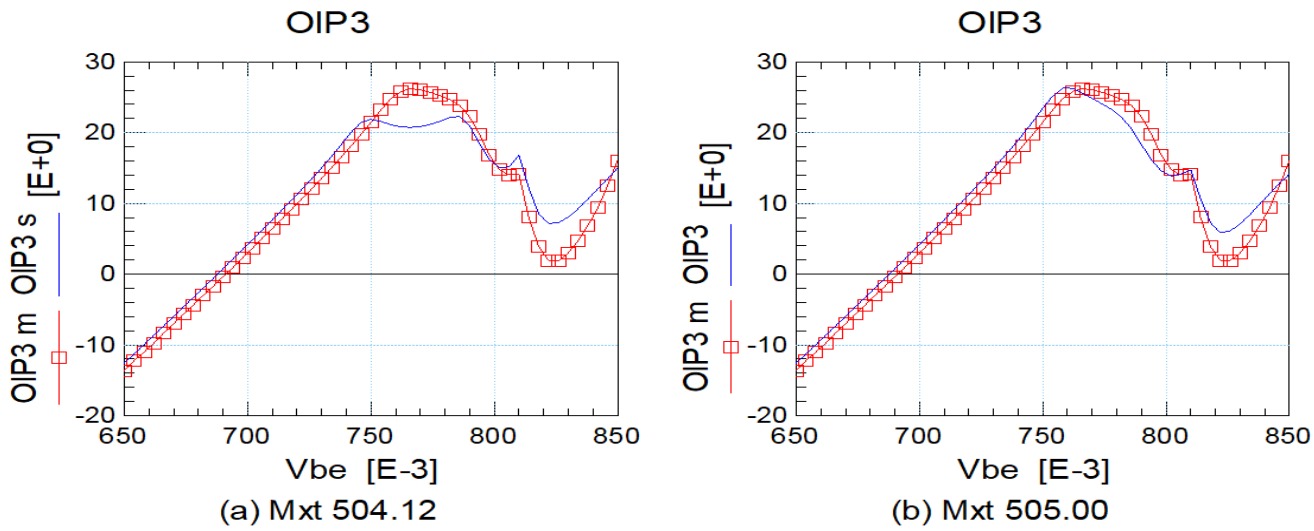

Figure 1.4: (a) IP3 versus V_{BE} simulated using Mextram 504.12 and measurement (b) IP3 versus V_{BE} simulated using Mextram 505.00 and measurement.

Mextram 504.12 does not have an accurate OIP3 simulation near peak IP3, but Mextram 505.00 provides a much better OIP3 simulation by modifying the intrinsic CB depletion capacitance. The differences of the intrinsic CB depletion capacitance between Mextram 504.12 and Mextram 505.00 are V_{junc} and V_{ch}. V_{junc} is the junction control voltage of the intrinsic CB depletion capacitance and V_{ch} is the control voltage smooth transition width. V_{junc} and V_{ch} in Mextram 504.12 will be introduced in chapter 2. Mextram 505.00 provides several options for V_{junc} and V_{ch}, and in Figure 1.4 (b) OIP3 simulation uses the default options of V_{junc} and V_{ch}. V_{junc} and V_{ch} in Mextram 505.00 will be introduced in chapter2. It is important to know why changing the intrinsic CB depletion capacitance can solve the distortion problem in OIP3. How the intrinsic CB depletion capacitance affects OIP3 will be studied in detail in chapter 4.

1.5 Summary

This chapter introduced the adventure of SiGe HBT, Mextram model, and some nonlinear concepts. Comparing OIP3 simulations between Mextram 504.12 with Mextram 505.00, Mextram 505.00 has a better OIP3 simulation by fixing the intrinsic CB depletion capacitance, which will be studied in great detail in the following chapters.

Chapter 2

V_{junc} and V_{ch} in Mextram 504.12 and 505.00

2.1 High Injection

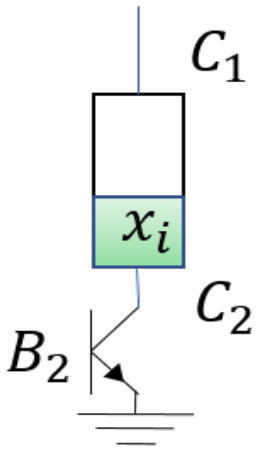

Figure 2.1: Simplified HBT configuration for high injection.

Figure 2.1 shows a simplified transistor model for high injection, C_1 is the external collector node, C_2 is the internal collector node, B_2 is the internal base node, and emitter is grounded. Epilayer is between nodes C_1 and C_2. x_i is the injection region in the epilayer.

Seeing from Figure 2.1, when $V_{B_2C_1}$ is zero, with current increasing, to much voltage drops on the epilayer, so that the internal $V_{B_2C_2}$ is under forward bias. High injection happens and the epilayer has an injection region. At some point, to be more precise when $V_{B_2C_2} \simeq V_{dC}$, these carrier densities become comparable to the back ground doping. From there on high-injection effects in the epilayer become important. This is the regime of quasi-saturation. All these affect epilayer resistance. Quasi-saturation means that when the voltage drop is due to an ohmic resistance, but also when it is due to a space-charge limited resistance, in which case the effect is also known as Kirk effect [4].

2.2 Intuitions of ohmic drift, SCR drift, ohmic QS and SCR QS

Consider fixing the reverse external CB junction bias $V_{C_1B_2} > 0$ and increasing $V_{B_2E_1}$ to increase collector current [4].

2.2.1 Low CB voltage

Assume $V_{C_1B_2}$ is low, e.g. 1V, so CB junction field is low, and there is no velocity saturation, at least at low current. The base side of the epilayer is depleted, by a width dependent on internal bias $V_{C_2B_2}$=$V_{C_1B_2}$-$I_{C_1C_2}R_{epi}$, as shown in Figure 2.2 (a). At low current, the rest of the epilayer simply behaves as an ohmic resistor, with a resistance dependent on the width of the charge neutral ohmic drift region. We denote this mode of epilayer operation *ohmic drift* [4].

At a sufficiently high current, the ohmic voltage drop is so large that $V_{C_2B_2}$ becomes sufficiently negative, corresponding to a forward internal junction bias $V_{B_2C_2}$ equal to built-in potential V_{dC}. CB junction depletion layer disappears, and the whole epilayer becomes charge neutral, with $n = N_{epi}$, as shown in Figure 2.2 (b). From ohm's law, the current at which ohmic quasi-saturation occurs can be estimated as $I_{qs,ohmic} \approx (V_{C_1B_2} + V_{dC})/R_{Cv}$, with R_{Cv} being the maximum resistance when the whole epilayer is ohmic [4].

With further increase of current, $V_{B_2C_2}$ essentially stays at V_{dC}. As $V_{B_2C_1}$ is fixed, epilayer voltage drop $V_{C_1C_2}$ stays the same, a further increase of current is physically made possible by a decrease of resistance, through shrink of the ohmic drift region width. An region with significant injection of carriers forms, as shown in Figure 2.2 (c). The drift region resistance is simply modified to $R_{Cv}(1 - x_i/W_{epi})$. We denote this mode of epilayer operation as *ohmic quasi-saturation*. The increase of x_i decreases resistance, allowing further current increase [4].

At some current, current density reaches $qN_{epi}v_{sat}$, the maximum ohmic drift value possible. Ohmic drift can no longer support further increase of current. Instead, electron density becomes greater than N_{epi} to allow a further current increase. As $n > N_{epi}$, space

charge region (SCR) forms near the end of the epilayer. The threshold current for this is denoted as I_{hc} in Mextram. This mode is denoted as *SCR quasi-saturation*, as shown in Figure 2.2 (d). A numerical example of how x_i increases with current at a low V_{C1B2} is shown in Figure 2.3 [4].

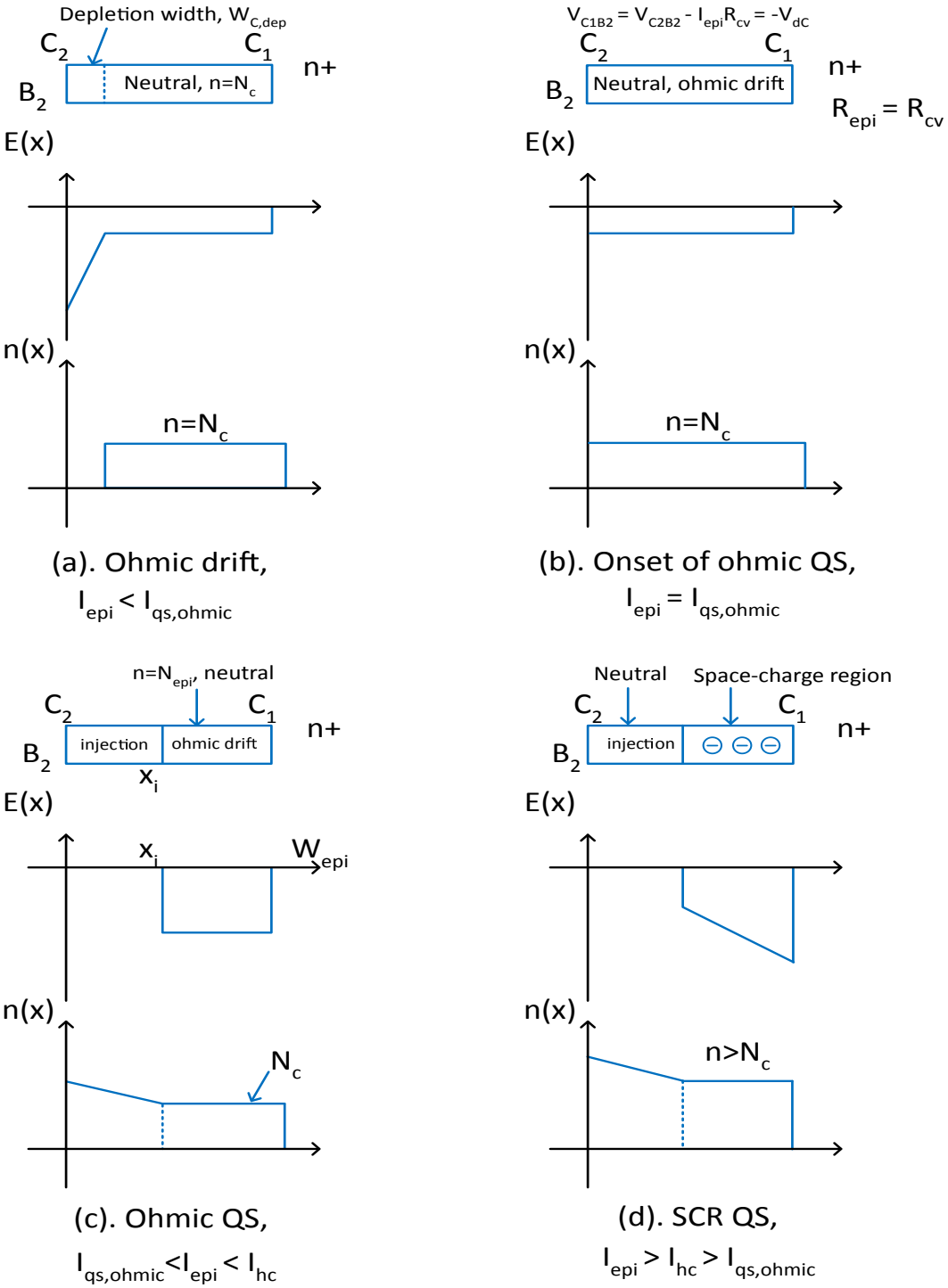

Figure 2.2: Epilayer state evolution with increasing current at a low V_{CB} [4].

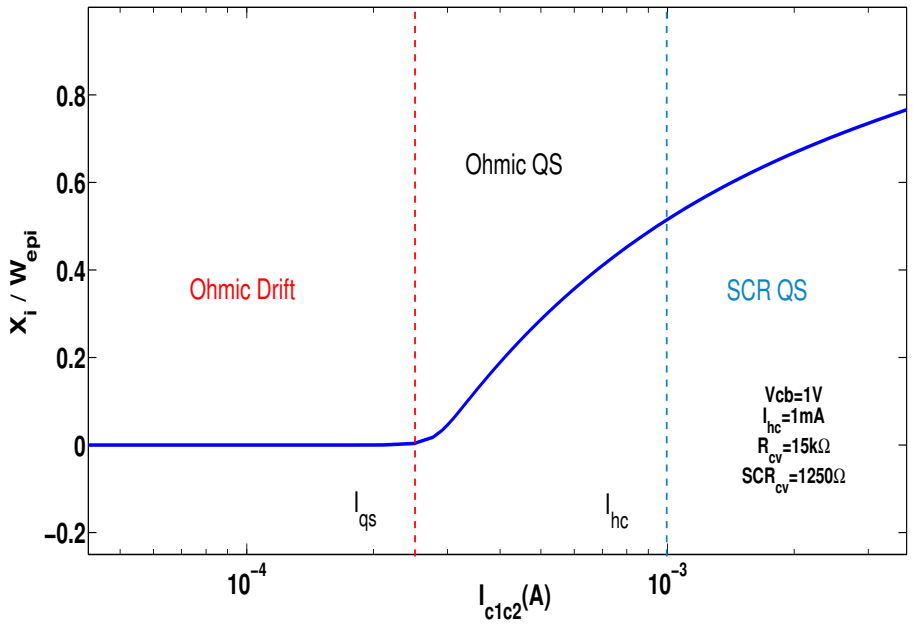

Figure 2.3: A numerical example of x_i/W_{epi} as a function of $I_{C_1C_2}$ at a low V_{CB} for a device with high R_{C_v} [4]

2.2.2 High CB voltage

The evolution of epilayer operation mode with increasing current described above occurs at relatively low external CB junction voltage, in devices with relatively high R_{Cv}, such as power devices, where the required I_{qs} is small compared to I_{hc}. This can also be easily seen from $I_{qs,ohmic} \approx (V_{C_1B_2} + V_{dC})/R_{Cv}$ [4].

At higher external CB junction voltage, or in devices with low R_{Cv}, ohmic quasi-saturation current is higher than I_{hc}, so that ohmic quasi-saturation never occurs. Instead, once current exceeds I_{hc}, electron density in the CB junction depletion layer exceeds background doping density N_{epi}, net charge density reverses polarity, causing a reversal of the electric field gradient. The whole epilayer has space charge, and electrons drift across the whole space charge layer at saturation velocity, with a resistance corresponding to that for space charge limited drift, SCR_{Cv}. We denote this epilayer operation mode *SCR drift* [4].

With further current increase, net charge density and hence field gradient increases. The field at the base end of the epilayer decreases, while the field at the buried layer end increases, to maintain the same total voltage drop. At some point, the field at base/epilayer junction decreases to a low enough value, 0 in classic treatment, the critical field required for velocity saturation in Mextram, injection of holes and electrons occur again, often referred to as "base push-out." A quasi neutral injection region forms near the base/epilayer junction, followed by a space charge region. We denote this as *SCR quasi-saturation*, which is better known as Kirk effect outside the Mextram world. An illustration of the operation mode evolution described above is given in Figure 2.4. A numerical example of how x_i increases with current at a high V_{C1B2} is shown in Figure 2.5 [4].

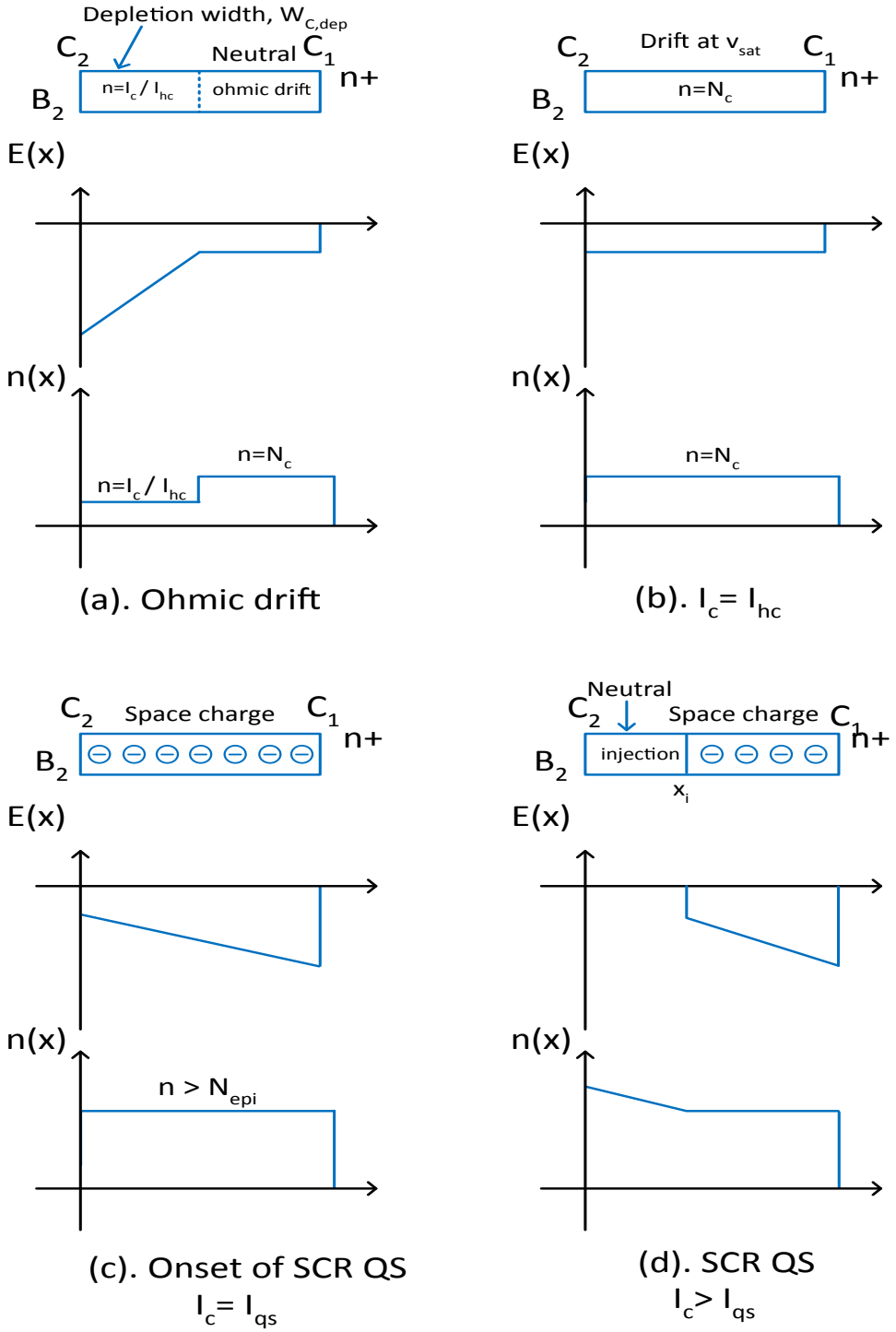

Figure 2.4: Epilayer state evolution with increasing current at a high V_{CB} [4].

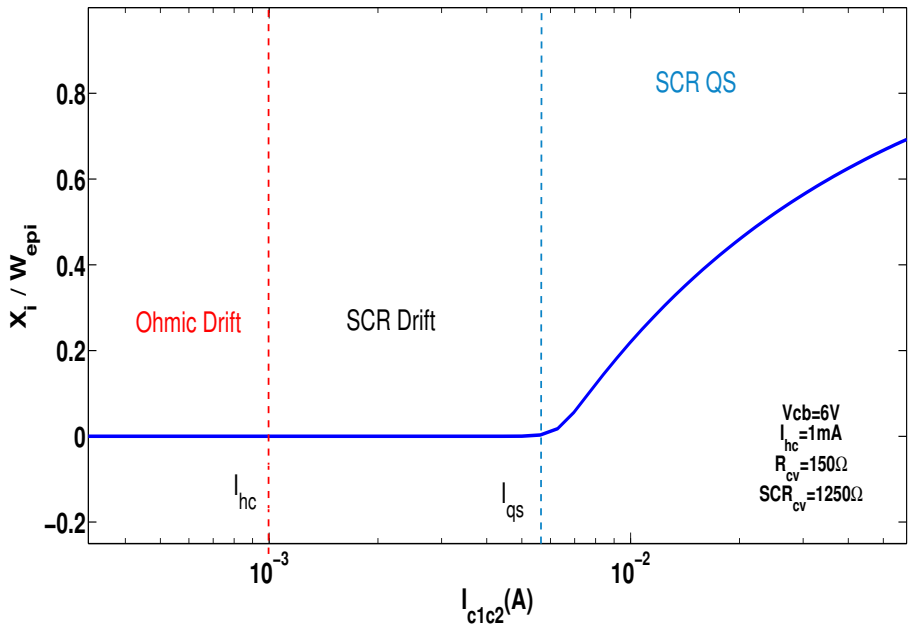

Figure 2.5: A numerical example of x_i/W_{epi} as a function of $I_{C_1C_2}$ at a high V_{CB} [4].

2.3 Epi-layer Model in Mextram

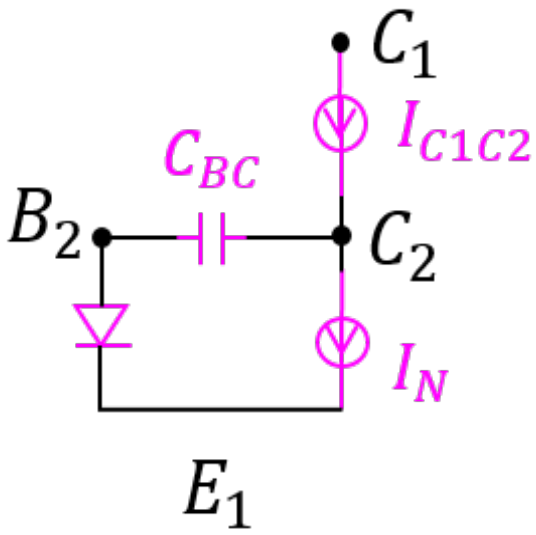

Figure 2.6: Simplified intrinsic circuit of HBT in Mextram.

Figure 2.6 shows a simplified intrinsic equivalent circuit of Mextram. Epilayer current $I_{C_1C_2}$ is from C_1 to C_2. Main current I_n is from C_2 to E_1, and intrinsic BC depletion capacitance is between B_2 and C_2.

In Mextram, the epilayer model is not used directly in epilayer to obtain the epilayer current $I_{C_1C_2}$, since the epilayer model has formulation $V_{B_2C_2} = f(I_{C_1C_2}, V_{B_2C_1})$, which cannot be used in circuit simulators to obtain $I_{C_1C_2}$. Mextram uses Kull model in epilayer for $I_{C_1C_2}$ and gives a internal base collector voltage $V_{B_2C_2}$ by the circuit simulator. Epilayer model is used to show all high injection effects of the epilayer current which is obtained by Kull model by giving another internal base collector voltage $V^*_{B_2C_2}$. Then $V^*_{B_2C_2}$ is used in mian current. The two internal base collector voltage has big differences. $V_{B_2C_2}$ is a bias that is given by the circuit simulator. This bias is used to calculate the current $I_{C_1C_2}$ through the epilayer, using the previously mentioned Kull model. It is therefore only a first step in the calculation and acts as a help variable. No physical meaning should be attached to it in forward mode. $V^*_{B_2C_2}$ is the bias that is in some sense the most physical one, since the effect

of quasi-saturation is taken into account. It is calculated using the external base collector bias $V_{B_2C_1}$ and the current $I_{C_1C_2}$ [6]. For the same intrinsic base collector junction, Mextram has two junction biases. A interesting question is how to choose internal BC junction voltage for the BC depletion capacitance.

2.4 V_{junc} and V_{ch} in Mextram 504.12

The junction voltage to be used for the intrinsic CB depletion capacitance must include the voltage drop over the epilayer. So instead of taking $V_{B_2C_1}$ as the voltage for calculating the depletion layer thickness, we use V_{junc}, which equals $V_{B_2C_1} + I_{C_1C_2}R_{Cv}$ for low currents [6].

In Mextram 504.12, we already mentioned that for small currents V_{junc} must equal $V_{B_2C_1} + I_{C_1C_2}R_{Cv}$. Furthermore, the point where for the capacitance a vanishing depletion width results ($V_{junc} \longrightarrow V_{d_C}$), is physically equal to the onset of quasi-saturation. It is very important to make sure that the same happens in this V_{junc} model. Hence the model needs $V_{junc} = V_{d_C}$, when $I_{C_1C_2} = I_{qs}$. I_{qs} is the quasi-saturation current. A logical choice would be to take $V_{junc} = V^*_{B_2C_2}$. There is however a catch to this [6].

Considering the total transit time, one of the contributions is due to the RC-time of the base-collector depletion capacitance and the (differential) resistance of the epilayer. The capacitance is fairly constant as function of current. The resistance, however, becomes very small once the transistor goes into quasi-saturation. This means that the contribution of this RC-time vanishes when the transistor is in quasi-saturation [6].

Let us consider the corresponding transit time in some more detail. We consider the Kirk effect,just before quasi-saturation. The depletion width is then equal to the epilayer width and the capacitance is given by $C = \varepsilon A_{em}/W_{epi}$. The partial resistance of the epilayer equals SCR_{Cv}. The contribution to the transit time is then

$$C \times SCR_{Cv} = \frac{W_{epi}}{2v_{sat}}, \tag{2.1}$$

a well-known expression. The time needed to cross the epilayer is the width divided by the velocity. The extra factor of 2 is a result from the electric field distribution which is triangular instead of flat. The corresponding charge will be given by:

$$Q \simeq \frac{I_{C_1C_2} W_{epi}}{2 v_{sat}}. \tag{2.2}$$

When injection starts, this charge will be modied. The effective space charge resistance will get an extra factor $(1 - \frac{x_i}{W_{epi}})^2$. This means that the charge now becomes

$$Q \simeq \frac{I_{C_1C_2} W_{epi}}{2 v_{sat}} (1 - \frac{x_i}{W_{epi}})^2. \tag{2.3}$$

In practice this means that the charge becomes nearly constant. The corresponding transit time, which is the derivative of the charge w.r.t. the current, then vanishes [6].

One way to prevent this in the model is to make sure that the effective epilayer resistance, in as far as it is used in this capacitance model, does not vanish once the transistor goes into quasi-saturation. Therefore V_{junc} should be an expression that is allowed to keep steadily increasing with current, even when $V_{junc} > V_{d_C}$. The effective voltage drop over the epilayer should be calculated [6]:

$$I_{C_1C_2} = \frac{V_{epi}}{SCR_{C_v}} \frac{V_{epi} + I_{hc} SCR_{C_v}}{V_{epi} + I_{hc} R_{C_v}}. \tag{2.4}$$

Here SCR_{C_v} is a parameter for epilayer space charge resistance and V_{epi} is the real voltage that drops over the epilayer. From this equation V_{epi} is a function of $I_{C_1C_2}$. Since it is used when $x_i > 0$, even though the equation only holds for $x_i = 0$, we call it $V_{x_i=0}$. The solution is given by [6]:

$$B_1 = \frac{1}{2} SCR_{C_v} (I_{C_1C_2} - I_{hc}), \tag{2.5}$$

$$B_2 = SCR_{C_v} RC_v I_{hc} I_{C_1C_2}, \tag{2.6}$$

$$V_{x_i=0} = B_1 + \sqrt{B_1^2 + B_2}. \tag{2.7}$$

The junction voltage is now the external voltage plus the voltage which drops over the epilayer [6]:

$$V_{junc} = V_{B_2C_1} + V_{x_i=0}. \tag{2.8}$$

In Mextram, intrinsic CB depletion capacitance is given by:

$$C_{t_C} = \frac{dQ_{t_C}}{dV_{junc}} = XC_{jc}C_{jc}((1 - X_p)\frac{f_I}{(1 - V_{junc}/V_{d_C})^{P_c}} + X_p), \tag{2.9}$$

$$f_I = (1 - \frac{I_{C_1C_2}}{I_{C_1C_2} + I_{hc}})^{m_C}, \tag{2.10}$$

where C_{t_C} is the intrinsic CB depletion capacitance, Q_{t_C} is the charge of the CB intrinsic capacitance, V_{junc} is the CB junction voltage, XC_{jc} is a parameter of the ratio between the extrinsic and the intrinsic CB capacitance, C_{jc} is a parameter of the CB capacitance at zero bias, V_{d_C} is a parameter of the CB diffusion voltage, X_P is a parameter of fraction of the CB depletion capacitance at large reverse bias, P_c is a parameter of the grading coefficient and f_I describes current effect on the CB depletion capacitance.

Eq. (2.9) gives a problem when $V_{junc} \geq V_{d_C}$. Hence a continuous formulation for capacitance is needed. It is not so important to have a physical description of depletion capacitance for $V_{junc} \geq V_{d_C}$ in forward bias. The diffusion charge in that region is much more important.

To avoid the problems, in Mextram the idea is to have an effective control voltage V_{jc} to replace V_{junc}. The effective voltage V_{jc} is a function:

$$V_{jc} = \begin{cases} V_{junc}, & V_{junc} \leq V_{FC} \\ V_{FC}, & V_{junc} > V_{FC} \end{cases}, \tag{2.11}$$

for $V_{junc} \leq V_{FC}$, $V_{jc} = V_{junc}$ and for $V_{junc} > V_{FC}$, $V_{jc} = V_{FC}$. V_{FC} is calculated such that the constant capacitance equals a factor a times the zero bias capacitance. V_{FC} is less than V_{d_C}. This V_{jc} makes capacitance as a junction capacitance when $V_{junc} \leq V_{FC}$ and a constant

when $V_{junc} > V_{FC}$ in high forward bias. Mextram uses a minlogexp function as the control voltage smooth limiting function:

$$V_{jc} = V_{junc} - V_{ch} \ln(1 + \exp[(V_{junc} - V_{FC})/V_{ch}]), \tag{2.12}$$

here, V_{ch} is the voltage smooth transition width.

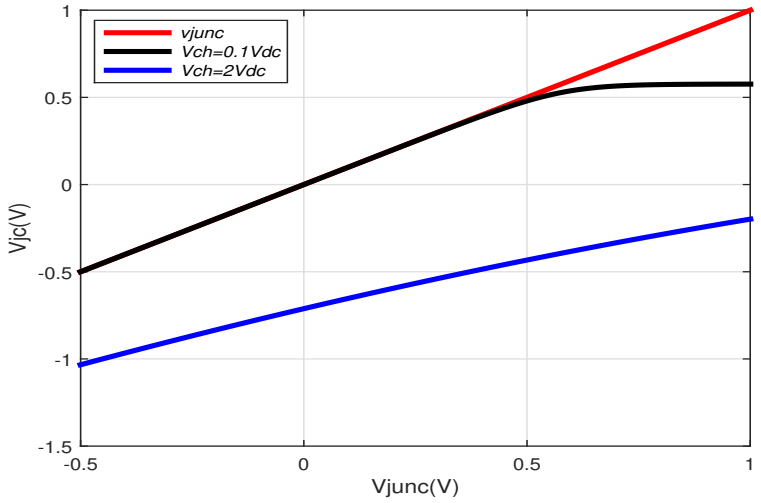

Figure 2.7: V_{jc} with different V_{ch} versus V_{junc}.

Figure 2.7 shows V_{jc}-V_{junc} with different V_{ch}. $0.1V_{ch}$ is the best choice for V_{ch}, and large V_{ch} distorts V_{jc}.

Mextram 504.12 does not use $V_{ch} = 0.1V_{d_C}$, which is used in Mextram 505.00 in forward mode, because this will give a much too steep increase from the zero-bias value to the constant value when due to quasi-saturation V_{junc} goes from negative values to values larger than the diffusion voltage V_{d_C}. To reduce this increase around quasi-saturation, Mextram 504.12 increases V_{ch} as quasi-saturation occurs:

$$V_{ch} = V_{dcctc}(0.1 + \frac{2I_{C_1C_2}}{I_{C_1C_2} + I_{qs}}). \tag{2.13}$$

Note that the current I_{qs} is used to determine when quasi-saturation starts.

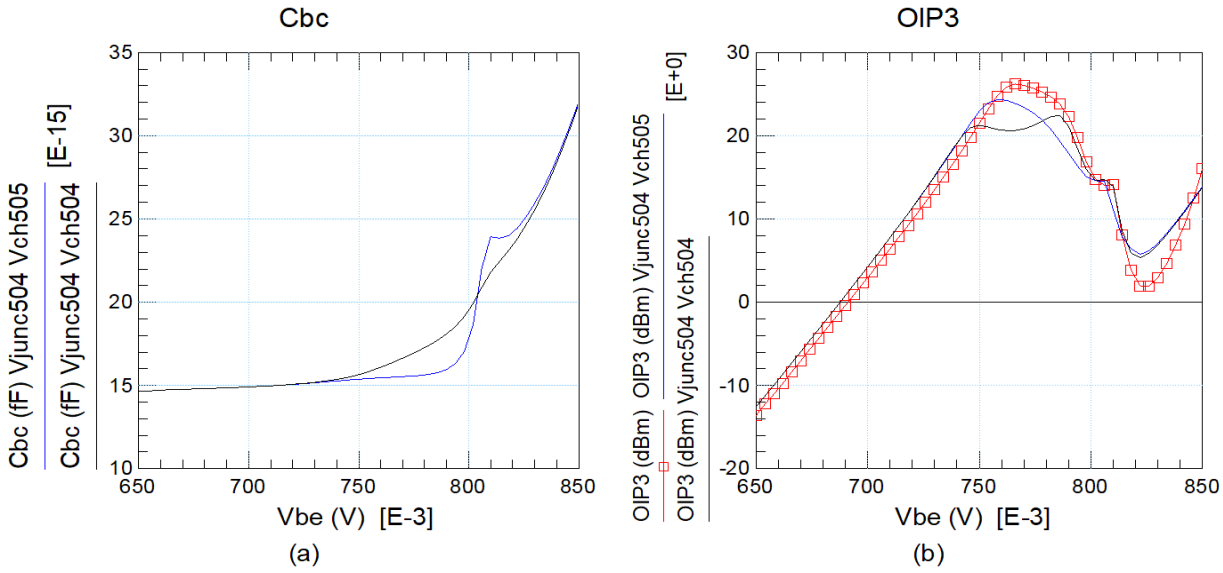

Figure 2.8: (a) Simulated C_{BC}-V_{BE} with Mextram 504.12 V_{junc} and Mextram 505.00 V_{ch} and simulated C_{BC}-V_{BE} with Mextram 504.12 V_{junc} and Mextram 504.12 V_{ch}. (b) Measured OIP3-V_{BE}, simulated OIP3-V_{BE} with Mextram 504.12 V_{junc} and Mextram 505.00 V_{ch} and simulated OIP3-V_{BE} with Mextram 504.12 V_{junc} and Mextram 504.12 V_{ch}.

Figure 2.8 (a) shows simulated C_{BC}-V_{BE} with Mextram 504.12 V_{junc} and Mextram 505.00 V_{ch} in blue and simulated C_{BC}-V_{BE} with Mextram 504.12 V_{junc} and Mextram 504.12 V_{ch} in black when $V_{CE} = 1.5V$ is fixed. Figure 2.8 (b) shows measured OIP3-V_{BE} in symbols, simulated OIP3-V_{BE} with Mextram 504.12 V_{junc} and Mextram 505.00 V_{ch} in blue and simulated OIP3-V_{BE} with Mextram 504.12 V_{junc} and Mextram 504.12 V_{ch} in black when $V_{CE} = 1.5V$ is fixed. It is clear that using Mextram 504.12 V_{junc} and Mextram 504.12 V_{ch} gives a smooth CB capacitance but a bad OIP3 near peak OIP3. Using Mextram 504.12 V_{junc} and Mextram 505.00 V_{ch} gives an abrupt BC capacitance but a good OIP3. It seems that the capacitance smooth and the peak OIP3 are determined by V_{ch}, but the main reason is V_{junc}, since how to choose V_{ch} depends on V_{junc}. In Mextram 504.12, V_{junc} goes up quickly once high injection happens, which needs an increasing V_{ch} to smooth junction voltage and the CB depletion capacitance. At high injection this V_{ch} equals to $2V_{d_C}$ which distorted V_{jc}

and the CB depletion capacitance. That means large V_{ch} will distort the CB capacitance and the peak OIP3 by V_{jc}.

2.5 Internal Voltages of HBT

When current increases into quasi-saturation, we want to see how the internal voltages varies in low injection and in high injection. x_i/W_{epi} should be shown to distinguish low injection and high injection. In low injection, x_i/W_{epi} is equal to zero, in high injection x_i/W_{epi} starts to grow up from 0 to 1.

Figure 2.9 shows I_C-V_{BE} and I_B-V_{BE} when V_{BC} is fixed to zero. Corresponding internal voltages are shown in Figure 2.10. Figure 2.10 shows V^*_{B2C2}-V_{BE}, V_{B2C2}-V_{BE}, V_{B2C1}-V_{BE} and Mextram 504.12 V_{junc}-V_{BE}, and x_i/W_{epi}-V_{BE} when V_{BC} is fixed to zero. When the current increases into quasi-saturation, V_{junc} of Mextram 504.12 increases fast once quasi-saturation occurs. V^*_{B2C2} has no meaning at low injection, so V^*_{B2C2} cannot be used as V_{junc}. In low injection V_{B2C2} is close to Mextram 504.12 V_{junc} and in high injection V_{B2C2} is close to V^*_{B2C2}, so V_{B2C2} can be an option for V_{junc}. If voltage drop over epilayer is neglected, V_{B2C1} can be used as V_{junc}. These two voltages will be V_{junc} options in Mextram 505.00.

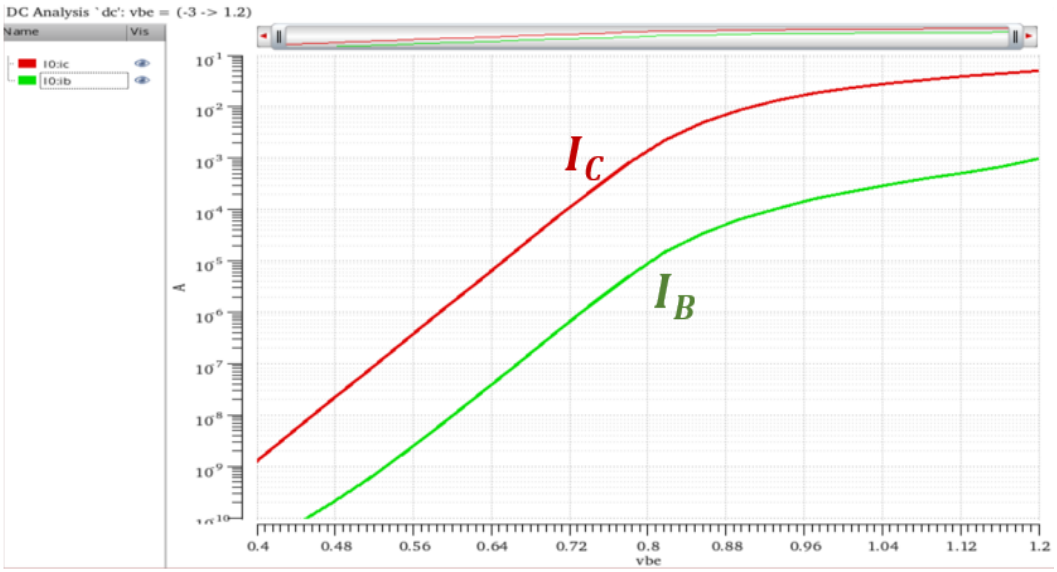

Figure 2.9: I_C and I_B versus V_{be}.

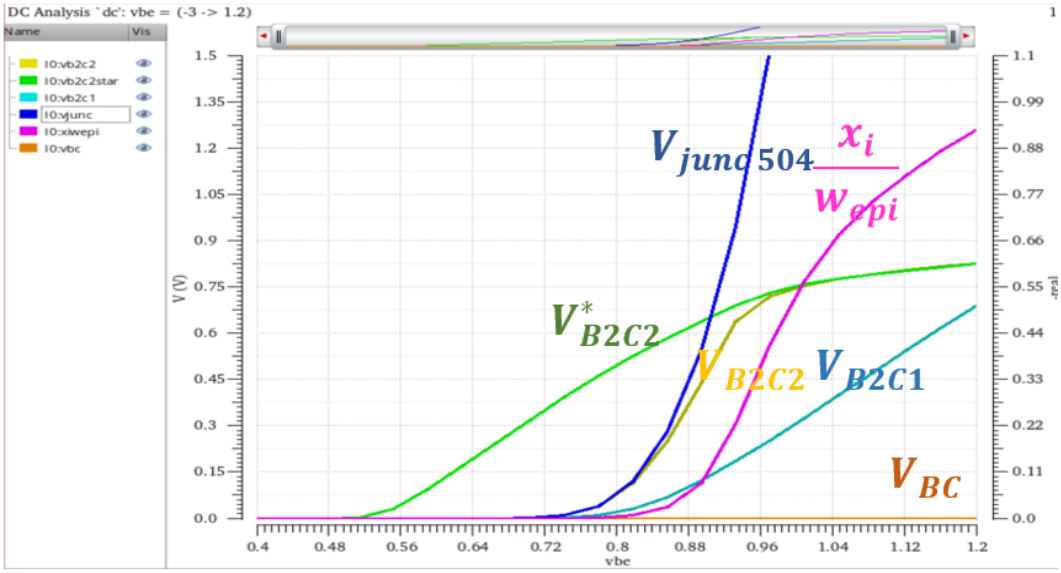

Figure 2.10: Internal voltages versus V_{be}.

2.6 V_{junc} and V_{ch} in Mextram 505.00

Mextram 505.00 provides several V_{junc} options for the intrinsic CB depletion capacitance. The CB depletion capacitance is important in low injection and in high injection diffusion capacitance is dominate. Neglecting the high injection and the voltage which drops over the epilayer, Mextram 505.00 gives another two V_{junc} options besides V_{junc} used in Mextram 504.12. V_{junc} options in Mextram 505.00 are given by:

$$swvjunc = 0 : V_{junc} = V_{B_2C_2}. \tag{2.14}$$

$$swvjunc = 1 : V_{junc} = V_{B_2C_1}. \tag{2.15}$$

$$swvjunc = 2 : V_{junc} = V_{B_2C_1} + V_{x_i0} \qquad \text{reduce to 504.12.} \tag{2.16}$$

Here $swvjunc$ is a switch parameter for BC junction control voltage V_{junc}. Mextram 505.00 also gives two V_{ch} options that are

$$swvchc = 0 : V_{ch} = 0.1V_{dcctc}. \tag{2.17}$$

$$swvchc = 1 : V_{ch} = V_{dcctc}(0.1 + \frac{2I_{C1C2}}{I_{C1C2} + I_{qs}}) \qquad \text{reduce to 504.12.} \tag{2.18}$$

Here $swvchc$ is a switch parameter for the voltage transition width V_{ch}, and V_{dcctc} is diffusion voltage for CB depletion capacitance in Mextram 505.00, like V_{d_C} in Mextram 504.12. $V_{junc} = V_{B_2C_2}$ and $V_{ch} = 0.1V_{vdcctc}$ are default junction voltage and default voltage transition width used in Mextram 505.00. Mextram 505.00 keeps V_{junc} and V_{ch} in Mextram 504.12 in its options. For the CB depletion capacitance effect on the RC-time, it can be fixed by other parameters in Mextram 505.00.

Figure 2.11 (a) shows simulated C_{BC}-V_{BE} with $swvjunc = 0$ $swvchc = 0$ in black, simulated C_{BC}-V_{BE} with $swvjunc = 1$ $swvchc = 0$ in blue and simulated C_{BC}-V_{BE} with $swvjunc = 2$ $swvchc = 0$ in pink using Mextram 505.00 when $V_{CE} = 1.5V$ is fixed. Figure 2.11 (b) shows measured OIP3-V_{BE}, simulated OIP3-V_{BE} with $swvjunc = 0$ $swvchc = 0$ in

black, simulated OIP3-V_{BE} with $swvjunc = 1$ $swvchc = 0$ in blue and simulated OIP3-V_{BE} with $swvjunc = 2$ $swvchc = 0$ in pink using Mextram 505.00 when $V_{CE} = 1.5V$ is fixed. Figure 2.11 (c) shows simulated V_{junc}-V_{BE} with $swvjunc = 0$ in black, simulated V_{junc}-V_{BE} with $swvjunc = 1$ in blue and simulated V_{junc}-V_{BE} with $swvjunc = 2$ in pink using Mextram 505.00 when $V_{CE} = 1.5V$ is fixed. It can be seen that when using Mextram 504.12 V_{junc}, the CB capacitance is not smooth and peak OIP3 is distorted, when using V_{junc} equals to $V_{B_2C_2}$ and $V_{B_2C_1}$, both CB capacitance are smooth and both OIP3 are much better near peak OIP3. Mextram 505.00 chooses $V_{junc} = V_{B_2C_2}$ and $V_{ch} = 0.1V_{dcctc}$ as its default values.

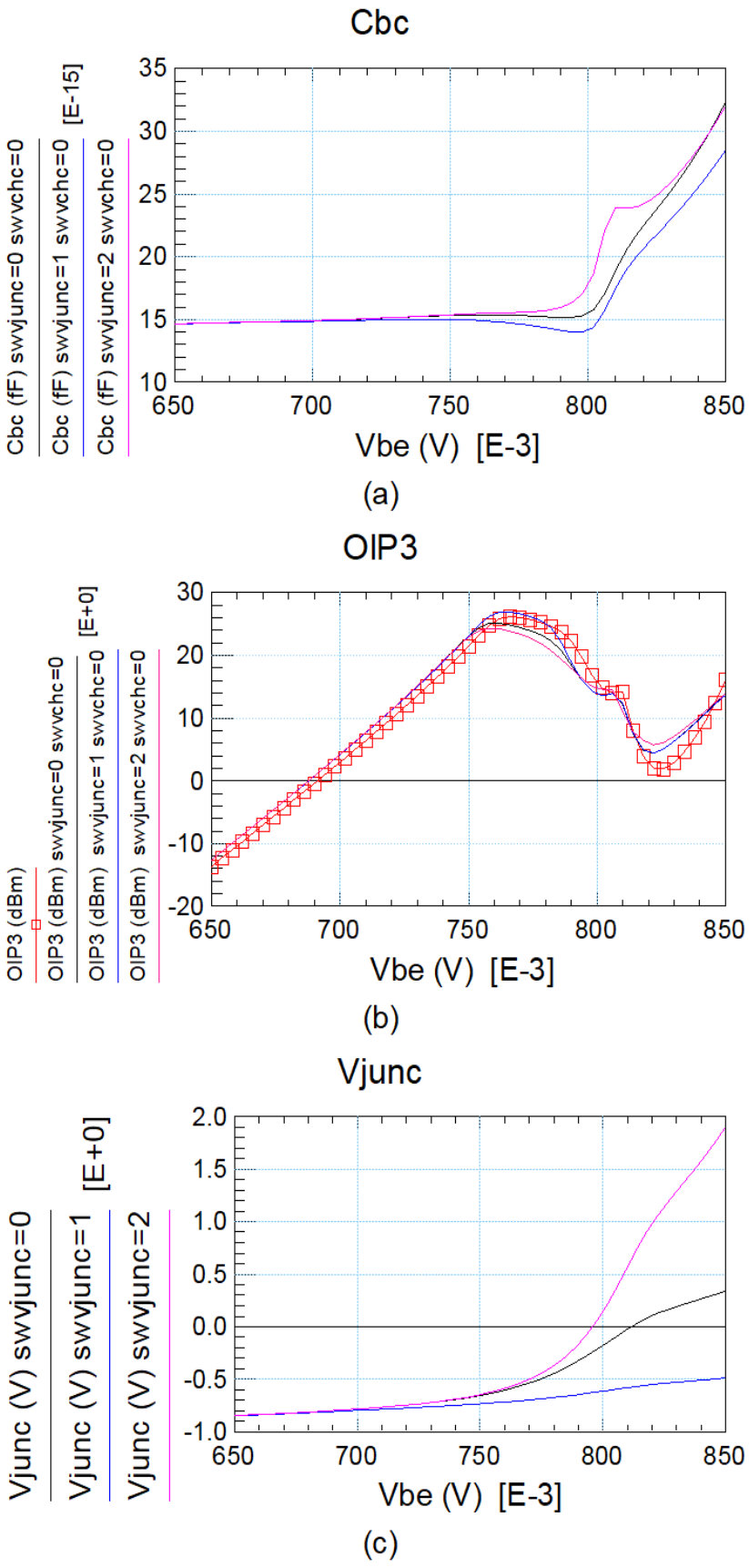

Figure 2.11: (a) Simulated C_{BC}-V_{BE} with $swvjunc = 0, 1, 2$ for $swvchc = 0$ using Mextram 505.00. (b) Simulated OIP3-V_{BE} with $swvjunc = 0, 1, 2$ for $swvchc = 0$ using Mextram 505.00. (C) Simulated V_{junc}-V_{BE} with $swvjunc = 0, 1, 2$ using Mextram 505.00.

2.7 Summary

This chapter introduced high injection in HBT, V_{junc} and V_{ch} in Mextram 504.12 and Mextram 505.00. In Mextram 504.12, V_{junc} is modeled by considering the epilayer voltage drop and the RC time constant of the intrinsic CB junction depletion capacitance, V_{ch} depends on V_{junc} for the voltage and the capacitance smooth. Mextram 505.00 provides two more V_{junc} and V_{ch} options. The effect on RC time constant from the capacitance can be fixed by some other parameters in Mextram 505.00. It is important that from Mextram 504.12 to Mextram 505.00 changing V_{junc} and V_{ch} can give a better OIP3 simulation. The main reason is that the V_{junc} in Mextram 504.12 goes up so quickly once high injection happens which distorted the peak OIP3. Changing CB depletion capacitance can improve OIP3 simulation, but it is important to know how the intrinsic CB depletion capacitance affects OIP3. That will be discussed in detail in the chapter 4.

Chapter 3

Mextram Intrinsic Base-Collector Depletion Capacitance

3.1 Intrinsic BC Depletion Capacitance in Mextram

In Mextram, intrinsic BC depletion capacitance is modeled by:

$$C_{t_C} = \frac{dQ_{t_C}}{dV_{junc}} = XC_{jc}C_{jc}((1 - X_p)\frac{f_I}{(1 - V_{jc}/V_{d_C})^{P_c}} + X_p), \tag{3.1}$$

$$f_I = (1 - \frac{I_{C_1C_2}}{I_{C_1C_2} + I_{hc}})^{m_C}, \tag{3.2}$$

where C_{t_C} is the intrinsic CB depletion capacitance, Q_{t_C} is the charge of the CB intrinsic capacitance, V_{junc} is the CB junction voltage, XC_{jc} is a parameter of the ratio between the extrinsic and the intrinsic CB capacitance, C_{jc} is a parameter of the CB capacitance at zero bias, V_{d_C} is a parameter of the BC diffusion voltage, X_P is a parameter of fraction of the CB depletion capacitance at large reverse bias, P_c is a parameter of the grading coefficient that has a theoretical value of 1/2 for an abrupt junction and 1/3 for a graded junction, and f_I describes current effect on the CB depletion capacitance.

Figure 3.1 shows C_{CB}-V, C_{CB} is the intrinsic CB depletion capacitance normalized to the zero bias value. At high forward bias, the capacitance is a constant. At middle bias, the capacitance grows up as V increasing. At large reverse bias, the capacitance looks like a constant, because considering the finite thickness of the epilayer, the capacitance cannot decrease too much.

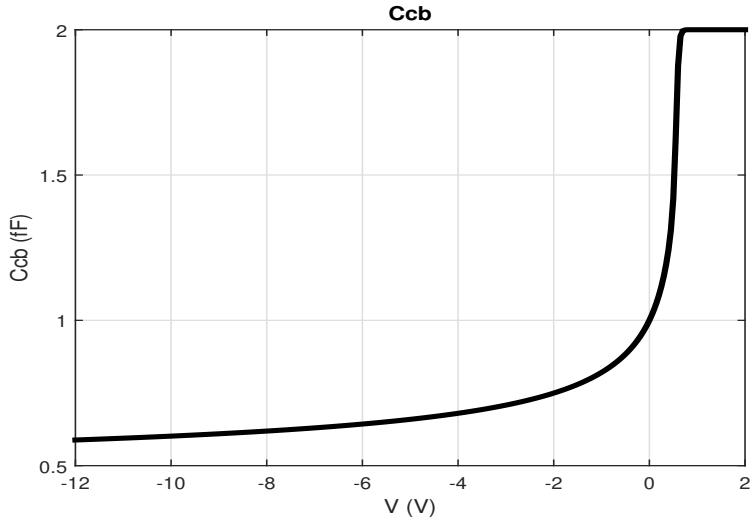

Figure 3.1: CB depletion capacitance versus V_{junc}

3.2 Fully Depleted Epi-layer Effect

The parameter X_p is used to describe the fully depleted epilayer effect. Considering a CB depletion capacitance in a bipolar transistor, the transistor actual structure should be taken into account. For collector base depletion capacitance, the finite thickness of the epilayer should be taken into account. For zero junction bias the capacitance equals in principle $C_{j0} = \epsilon_{si}/x_{d0}$. Here x_{d0} is the width of the depletion region in the epilayer at zero bias. When the junction becomes strongly reverse biased the depletion layer will be wider than the epilayer. Since the buried layer has a much higher doping, the width of the depletion layer will not increase much beyond the width of the epilayer W_{epi} (reach-through). From there on, the capacitance will be approximately constant, with a value of in principle ϵ_{si}/W_{epi}. This behavior will be approximated by taking the total capacitance as a sum of a constant part in large reverse bias and a junction part in middle and high forward bias. The parameter is given by $X_p = x_{d0}/W_{epi}$ [6]. The difference between capacitances with reach-through and without reach-through is shown in Figure 3.2.

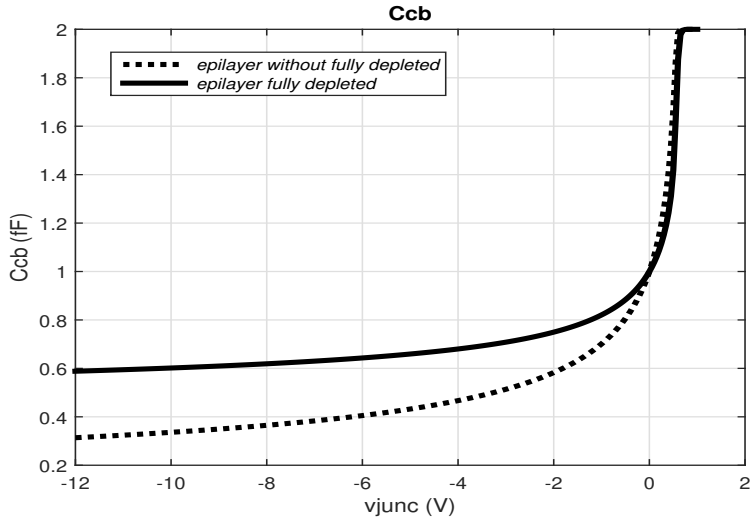

Figure 3.2: C_{CB}-V with or without fully depleted epi-layer effect.

Figure 3.2 shows C_{CB}-V with epilayer fully depleted effect for parameters $C_{jc} = 1$, $Pc = 0.4$, $V_{d_C} = 0.7V$,$X_p = 0.4$. The different curves are for the capacitance without reach-through (dotted), and the capacitance with reach-through (solid). At large reverse bias, the parameter X_p makes the capacitance as a constant and drop less.

3.3 Current Dependence

Next the current dependence in BC depletion capacitance will be discussed. This effect is modeled by the factor f_I in equation (3.2). In equation (3.2), $I_{C_1C_2}$ is the epilayer current, I_{hc} is a parameter of current for velocity saturation in the epilayer, m_C is a parameter of coefficient for current modulation of CB depletion capacitance. The depletion thickness changes due to the charge of electrons moving. Since the base layer has a much higher doping than epilayer, the base depletion width can be negligible, and the depletion thickness in epilayer should be taken into account. In general, without current effect the depletion width is $x_d = \sqrt{2\varepsilon_{si}(V_{dc} - V_f)/(qN_{epi})}$. Here V_f is applied bias, and N_{epi} is epilayer doping that is also depletion charge concentration.

Considering the current effect and assuming the electrons moving through depletion region at the saturated velocity v_{sat}, the effective charge in the depletion thickness is $Q_{eff} = N_{epi} - I_{C_1C_2}/qv_{sat}$. Hence the depletion width is

$$x_d = \sqrt{\frac{2\varepsilon_{si}(V_{d_C} - V_f)}{q(N_{epi} - \frac{I_{C_1C_2}}{qv_{sat}})}}, \tag{3.3}$$

then

$$x_d = \sqrt{\frac{2\varepsilon(V_{d_C} - V_f)}{qN_{epi}(1 - \frac{I_{C_1C_2}}{I_{hc}})}}, \tag{3.4}$$

here we define $I_{hc} = qv_{sat}N_{epi}$.

Current dependence mainly describes that the variation of CB depletion width depends on epilayer current, since the current changes the effective charge in the depletion region. The epilayer current also gives a voltage drop over epilayer, which impacts on V_{jumc}.

3.4 Summary

This chapter introduced intrinsic CB depletion capacitance in Mextram. Current dependence and fully depleted epilayer effect of the intrinsic CB capacitance are discussed.

Chapter 4

OIP3 in Common Emitter Configuration

The linearity characteristics of a SiGe HBT operating in a common-emitter (CE) configuration are addressed. Mextram 505.00 provides several options for modeling V_{junc} and V_{ch}, and gives a much better OIP3 simulation than Mextram 504.12. This chapter will figure out how different V_{junc} and V_{ch} affect OIP3 in Mextram 504.12 and Mextram 505.00. In this chapter all measurements and all simulations are in common emitter configuration when $V_{CE} = 1.5V$.

4.1 OIP3 simulation using Mextram 504.12 and Mextram 505.00

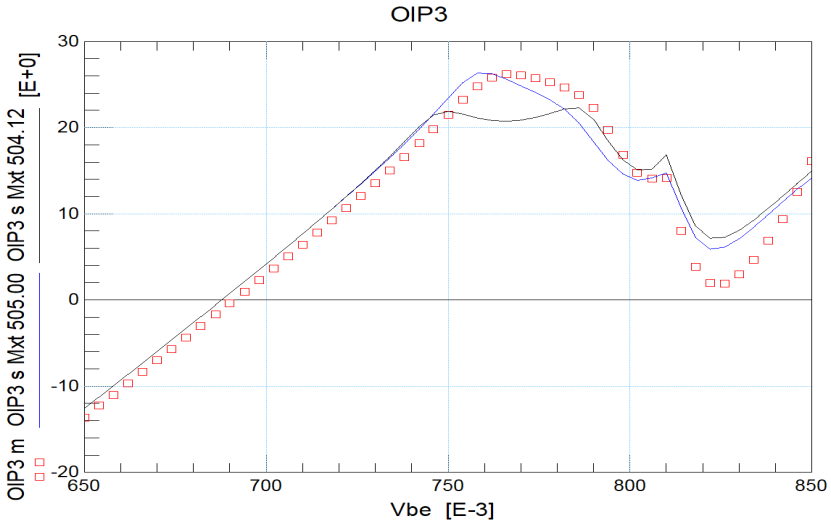

Figure 4.1: Measured OIP3 and simulated OIP3 using Mextram 504.12 and 505.00 across V_{BE}.

Figure 4.1 shows measured OIP3 together with simulated OIP3 using Mextram 504.12 and 505.00 versus V_{BE}. The blue line is OIP3 simulation using Mextram 505.00, the black

line is OIP3 simulation using Mextram 504.12 and the red symbol is OIP3 measurement. Mextram 505.00 provides a much better OIP3 simultion than Mextram 504.12 near peak OIP3. The difference between Mextram 504.12 and Mextram 505.00 is intrinsic CB depletion capacitances C_{tci}, and C_{tci} has a big impact on OIP3. It is important to know how C_{tci} affects OIP3.

4.2 First and Third Order Output Currents Effect on OIP3

OIP3 is determined by the currents magnitude ratio $|I_{out,3rd}/I_{out,1st}|$ of the third order output current $I_{out,3rd}$ to the first order output current $I_{out,1st}$:

$$P_{out,3rd} = I_{out,3rd}^2 R_{out}, \tag{4.1}$$

$$P_{out,1st} = I_{out,1st}^2 R_{out}, \tag{4.2}$$

$$IM3 = \sqrt{\frac{P_{out,3rd}}{P_{out,1st}}} = \frac{|I_{out,3rd}|}{|I_{out,1st}|}, \tag{4.3}$$

$$OIP3 = P_{out,1st} - \frac{1}{2} IM3|_{dB}. \tag{4.4}$$

In Figure 4.2 (a1) (a2) (b1) (b2), the blue lines are simulations and the red symbols are measurement. Figure 4.2 (a1) shows measured $|I_{out,3rd}/I_{out,1st}|$ and simulated $|I_{out,3rd}/I_{out,1st}|$ using Mextram 505.00 versus V_{BE}, and Figure 4.2 (a2) shows measured OIP3 and simulated OIP3 using Mextram 505.00 versus V_{BE}. Figure 4.2 (b1) shows measured $|I_{out,3rd}/I_{out,1st}|$ and simulated $|I_{out,3rd}/I_{out,1st}|$ using Mextram 504.12 versus V_{BE}, and Figure 4.2 (b2) shows measured OIP3 and simulated OIP3 using Mextram 504.12 versus V_{BE}. Comparing Figure 4.2 (a1) (b1) with Figure 4.2 (a2) (b2), for both measurement and simulation peak OIP3 occurs where $|I_{out,3rd}/I_{out,1st}|$ is minimized as expected. This implies $|I_{out,3rd}/I_{out,1st}|$ difference depends on C_{tci} difference and then causes different peak OIP3 in Mextram 505.00 and

Mextram 504.12. It is important to know how C_{tci} affects $|I_{out,3rd}/I_{out,1st}|$. So $|I_{out,1st}|$ and $|I_{out,3rd}|$ of the two cases should be compared.

In Figure 4.3 (a) (b) (c) (d), the blue lines are simulations using Mextram 505.00, the black lines are simulations using Mextram 504.12 and the red symbols are measurement. Figure 4.3 (a) shows measured OIP3-V_{BE} together with simulated OIP3-V_{BE} using Mextram 504.12 and 505.00. Figure 4.3 (b) shows measured $|I_{out,1st}|$-V_{BE} together with simulated $|I_{out,1st}|$-V_{BE} using Mextram 504.12 and 505.00. Figure 4.3 (c) shows measured $|I_{out,3rd}|$-V_{BE} and simulated $|I_{out,3rd}|$-V_{BE} using Mextram 504.12 and 505.00. Figure 4.3 (d) shows measured $|I_{out,3rd}/I_{out,1st}|$-$V_{BE}$ and simulated $|I_{out,3rd}/I_{out,1st}|$-$V_{BE}$ using Mextram 504.12 and 505.00. The $|I_{out,3rd}/I_{out,1st}|$ difference near peak OIP3 mainly depends on $|I_{out,3rd}|$, since $|I_{out,1st}|$ are almost the same near peak OIP3. This implies peak OIP3 is mainly determined by the minimized third order output current. It should be discussed that how the real part and the imaginary part of $I_{out,3rd}$ impact peak OIP3.

In Figure 4.4 (a1) (a2) (b1) (b2), lines show simulations and symbols show measurements. Figure 4.4 (a1) shows simulated real($I_{out,3rd}$)-V_{BE} in red, simulated imag($I_{out,3rd}$)-V_{BE} in blue, and simulated $|I_{3rd}|$-V_{BE} in purple using Mextram 505.00. Figure 4.4 (a2) shows measured OIP3-V_{BE} and simulated OIP3-V_{BE} using Mextram 505.00. Figure 4.4 (b1) shows simulated real($I_{out,3rd}$)-V_{BE} in red, simulated imag($I_{out,3rd}$)-V_{BE} in blue, and simulated $|I_{3rd}|$-V_{BE} in purple using Mextram 504.12. Figure 4.4 (b2) shows measured OIP3-V_{BE} and simulated OIP3-V_{BE} using Mextram 504.12. Seeing Figure 4.4 (a1) and Figure 4.4 (b1), the minimum magnitude of $I_{out,3rd}$ depends on both real and imaginary part of $I_{out,3rd}$. Comparing Figure 4.4 (a1) with Figure 4.4 (a2) and comparing Figure 4.4 (b1) with Figure 4.4 (b2), the bias where peak OIP3 happens mainly depends on imaginary part of $I_{out,3rd}$. For the two cases peak OIP3 is determined by both real and imaginary part of $I_{out,3rd}$, and peak OIP3 bias mainly depends on the imaginary part of $I_{out,3rd}$.

$I_{out,3rd}$ is the third order output current, and in HBT device, the output current consists of several internal component currents. It is necessary to see each component current to find out which one affects peak OIP3.

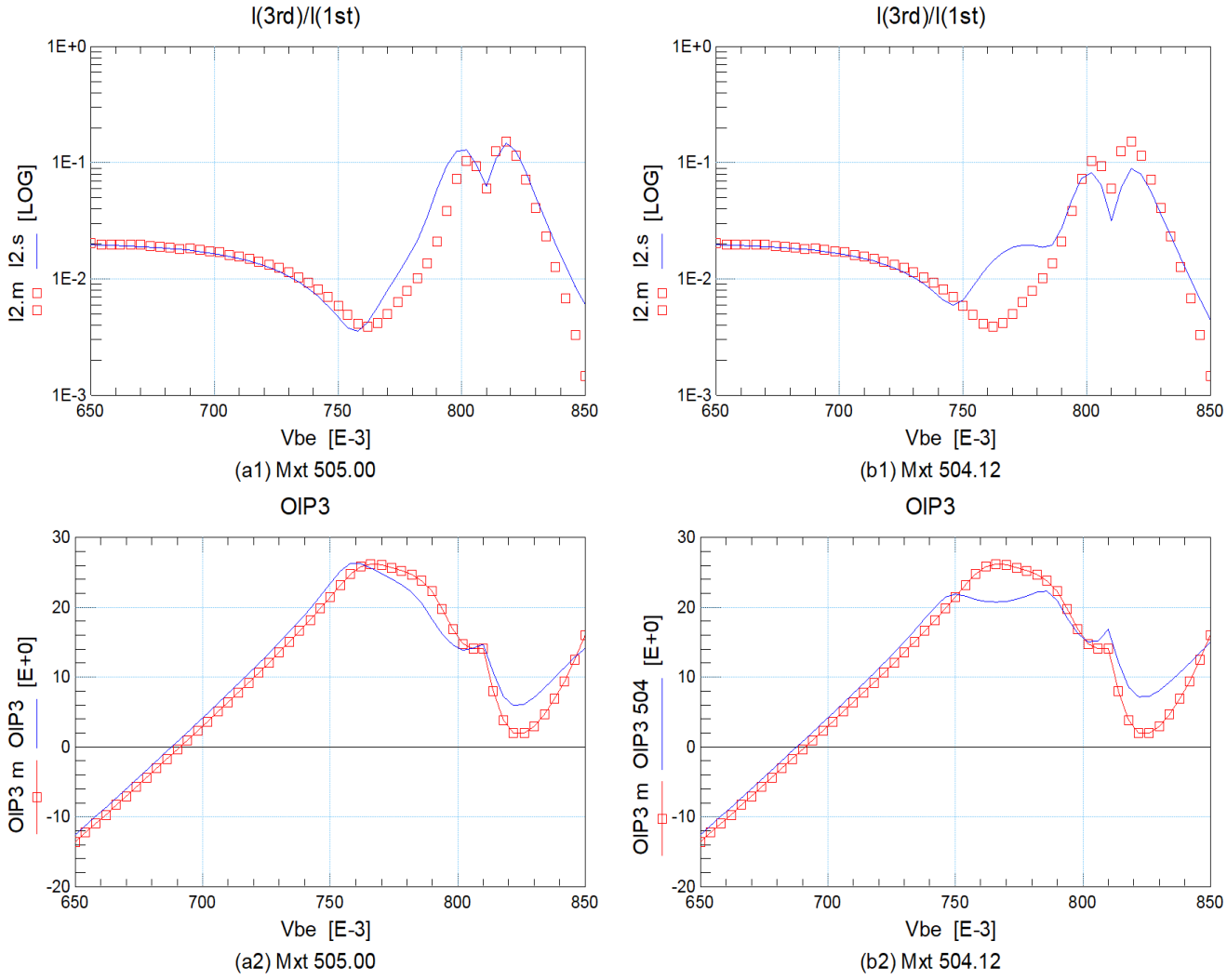

Figure 4.2: (a1) Measured $|I_{out,3rd}/I_{out,1st}|$ and simulated $|I_{out,3rd}/I_{out,1st}|$ using Mextram 505.00 versus V_{BE}. (a2) Measured OIP3 and simulated OIP3 using Mextram 505.00 versus V_{BE}. (b1) Measured $|I_{out,3rd}/I_{out,1st}|$ and simulated $|I_{out,3rd}/I_{out,1st}|$ using Mextram 504.12 versus V_{BE}. (b2) Measured OIP3 and simulated OIP3 using Mextram 504.12 versus V_{BE}.

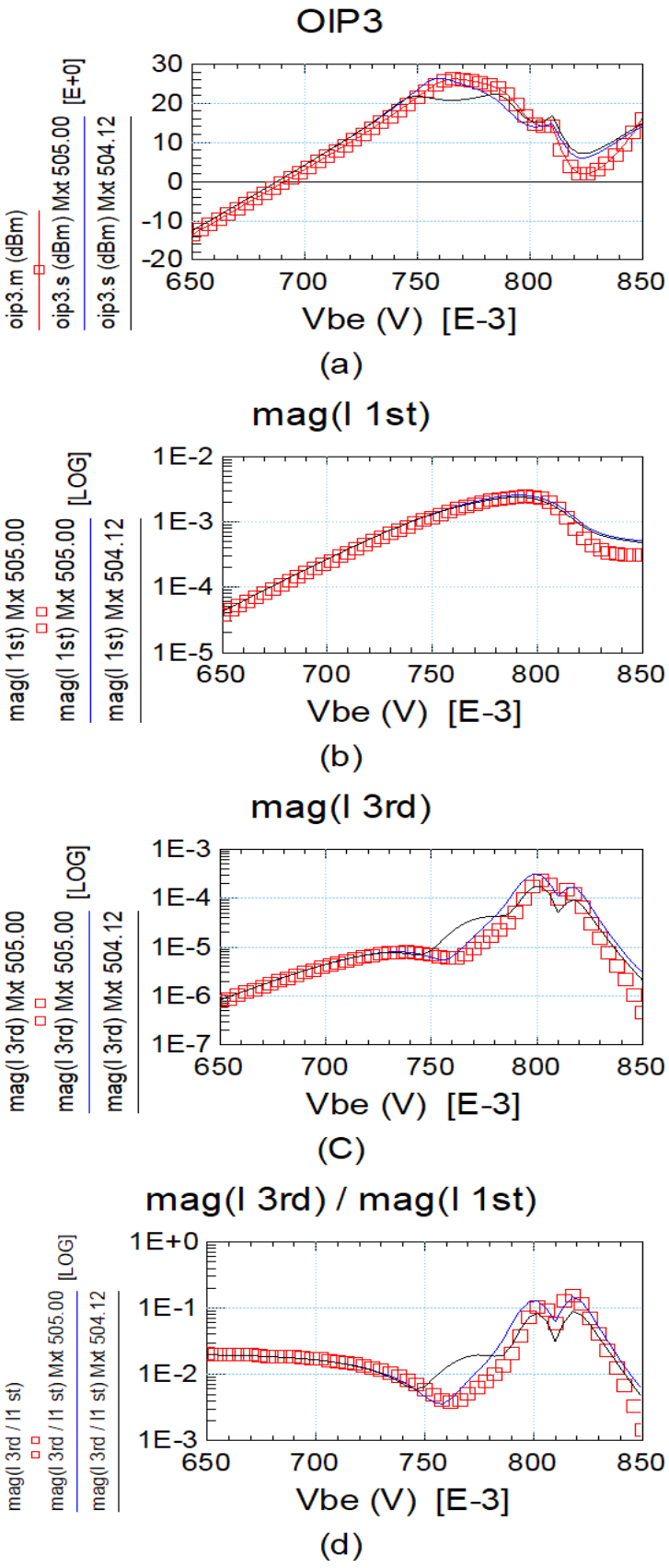

Figure 4.3: (a) Measured OIP3 and simulated OIP3 using Mextram 504.12 and 505.00 versus V_{BE}. (b) Measured $|I_{out,1st}|$ and simulated $|I_{out,1st}|$ using Mextram 504.12 and 505.00 versus V_{BE}. (c) Measured $|I_{out,3rd}|$ and simulated $|I_{out,3rd}|$ using Mextram 504.12 and 505.00 versus V_{BE}. (d) Measured $|I_{out,3rd}/I_{out,1st}|$ and simulated $|I_{out,3rd}/I_{out,1st}|$ using Mextram 504.12 and 505.00 versus V_{BE}.

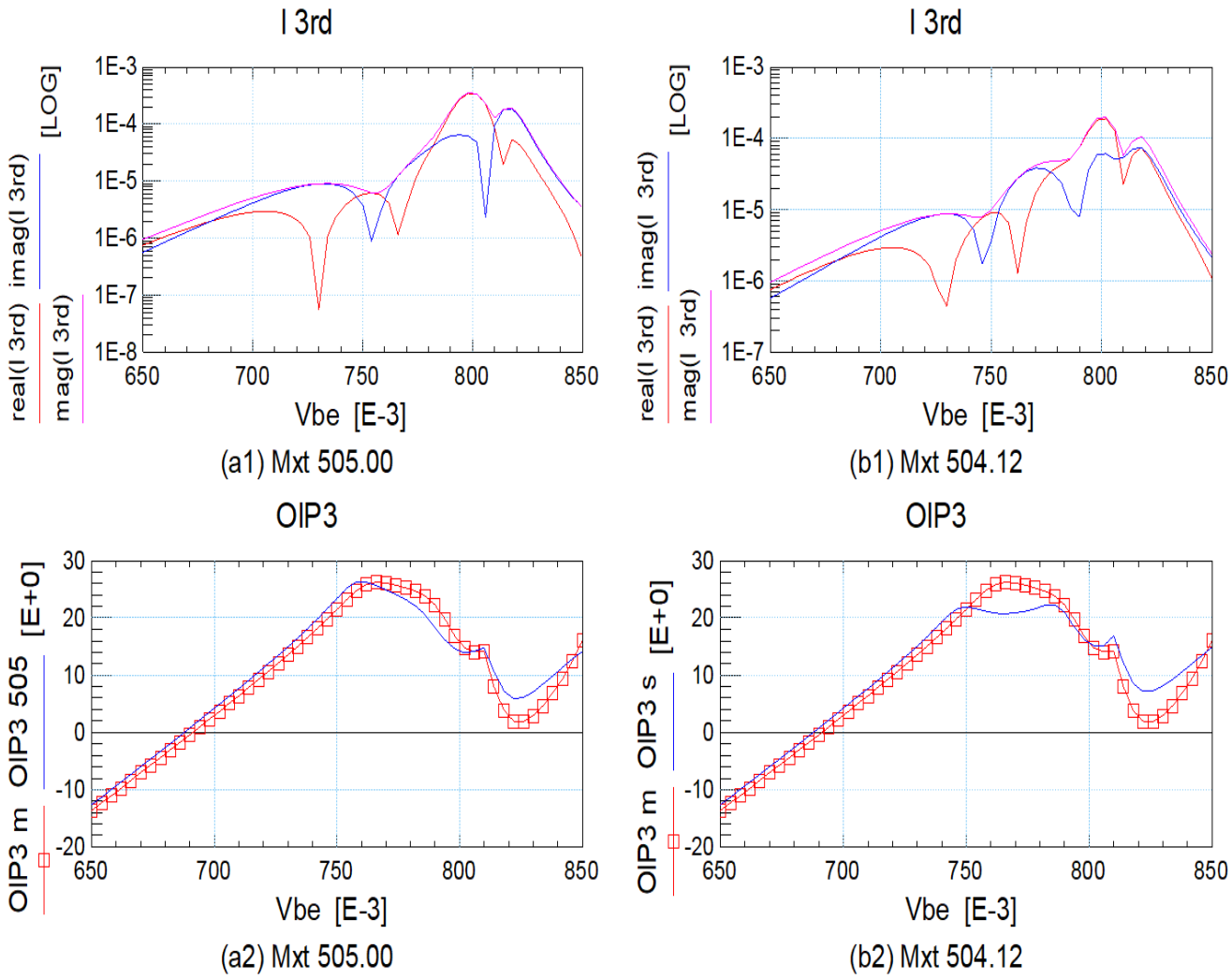

Figure 4.4: (a1) Simulated real($I_{out,3rd}$), simulated imag($I_{out,3rd}$) and simulated mag($I_{out,3rd}$) using Mextram 505.00 versus V_{BE}. (a2) Measured OIP3 and simulated OIP3 using Mextram 505.00 versus V_{BE}. (b1) Simulated real($I_{out,3rd}$), simulated imag($I_{out,3rd}$) and simulated mag($I_{out,3rd}$) using Mextram 504.12 versus V_{BE}. (b2) Measured OIP3 and simulated OIP3 using Mextram 504.12 versus V_{BE}.

4.3 Third Order Component Currents

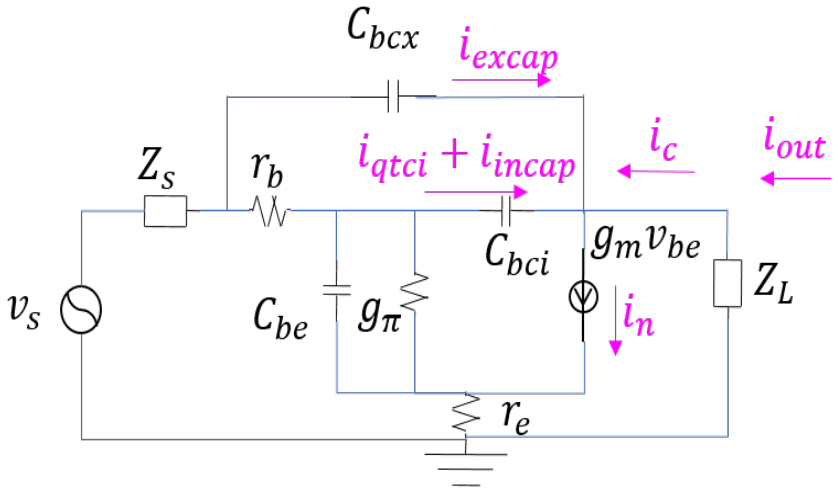

Figure 4.5: Simplified equivalent circuit of an HBT.

Figure 4.5 shows a simplified equivalent circuit of an HBT without pads. Seeing Figure 4.5, the collector current i_c

$$i_c = i_n - i_{qtci} - i_{incap} - i_{excap}, \tag{4.5}$$

relates to i_n, the main current, i_{qtci}, the dynamic current of the intrinsic CB depletion capacitance, i_{incap}, the dynamic current of the intrinsic CB diffusion capacitance, and i_{excap}, the dynamic current of the extrinsic CB capacitance including depletion and diffusion capacitances. i_{out}, the output current that is measured, differs from i_c by a small amount, due to pads. Blow we use i_c to approximate i_{out}.

In Figure 4.6 (a1) (a2) (b1) (b2), lines show simulations and symbols show measurements. Figure 4.6 (a1) shows real part measurement of $i_{out,3rd}$-V_{BE} and real part simulations of $i_{out,3rd}$-V_{BE} in blue, $i_{c,3rd}$-V_{BE} in black, $i_{n,3rd}$-V_{BE} in pink, $i_{qtci,3rd}$-V_{BE} in green, $i_{incap,3rd}$-V_{BE} in yellow, $i_{excap,3rd}$-V_{BE} in purple, using Mextram 505.00. Figure 4.6 (a2) shows imaginary part measurement of $i_{out,3rd}$-V_{BE} and imaginary part simulations of $i_{out,3rd}$-V_{BE} in blue, $i_{c,3rd}$-V_{BE} in black, $i_{n,3rd}$-V_{BE} in pink, $i_{qtci,3rd}$-V_{BE} in green, $i_{incap,3rd}$-V_{BE} in yellow, $i_{excap,3rd}$-V_{BE} in purple, using Mextram 505.00. Figure 4.6 (b1) shows real part measurement of $i_{out,3rd}$-V_{BE} and real part simulations of $i_{out,3rd}$-V_{BE} in blue, $i_{c,3rd}$-V_{BE} in black, $i_{n,3rd}$-V_{BE} in pink, $i_{qtci,3rd}$-V_{BE} in green, $i_{incap,3rd}$-V_{BE} in yellow, $i_{excap,3rd}$-V_{BE} in purple, using Mextram 504.12. Figure 4.6 (b2) shows imaginary part measurement of $i_{out,3rd}$-V_{BE} and imaginary part simulations of $i_{out,3rd}$-V_{BE} in blue, $i_{c,3rd}$-V_{BE} in black, $i_{n,3rd}$-V_{BE} in pink, $i_{qtci,3rd}$-V_{BE} in green, $i_{incap,3rd}$-V_{BE} in yellow, $i_{excap,3rd}$-V_{BE} in purple, using Mextram 504.12. Comparing simulated $i_{out,3rd}$ with simulated $i_{c,3rd}$, for both real part and imaginary part $i_{c,3rd}$ is close to $i_{out,3rd}$, we use $i_{c,3rd}$ to approximate $i_{out,3rd}$ for Mextram 504.12 and 505.00. Comparing $i_{c,3rd}$ with individual components $i_{n,3rd}$, $i_{qtci,3rd}$, $i_{excap,3rd}$ and $i_{incap,3rd}$ in Mextram 504.12 and 505.00, for $i_{out,3rd}$, $i_{n,3rd}$ dominates in both real and imaginary part near peak OIP3. This implies in Mextram 504.12 and 505.00 different C_{tci} mainly affect component current $i_{n,3rd}$ to give different peak OIP3. It should be clear that how the intrinsic CB depletion capacitance affects $i_{n,3rd}$.

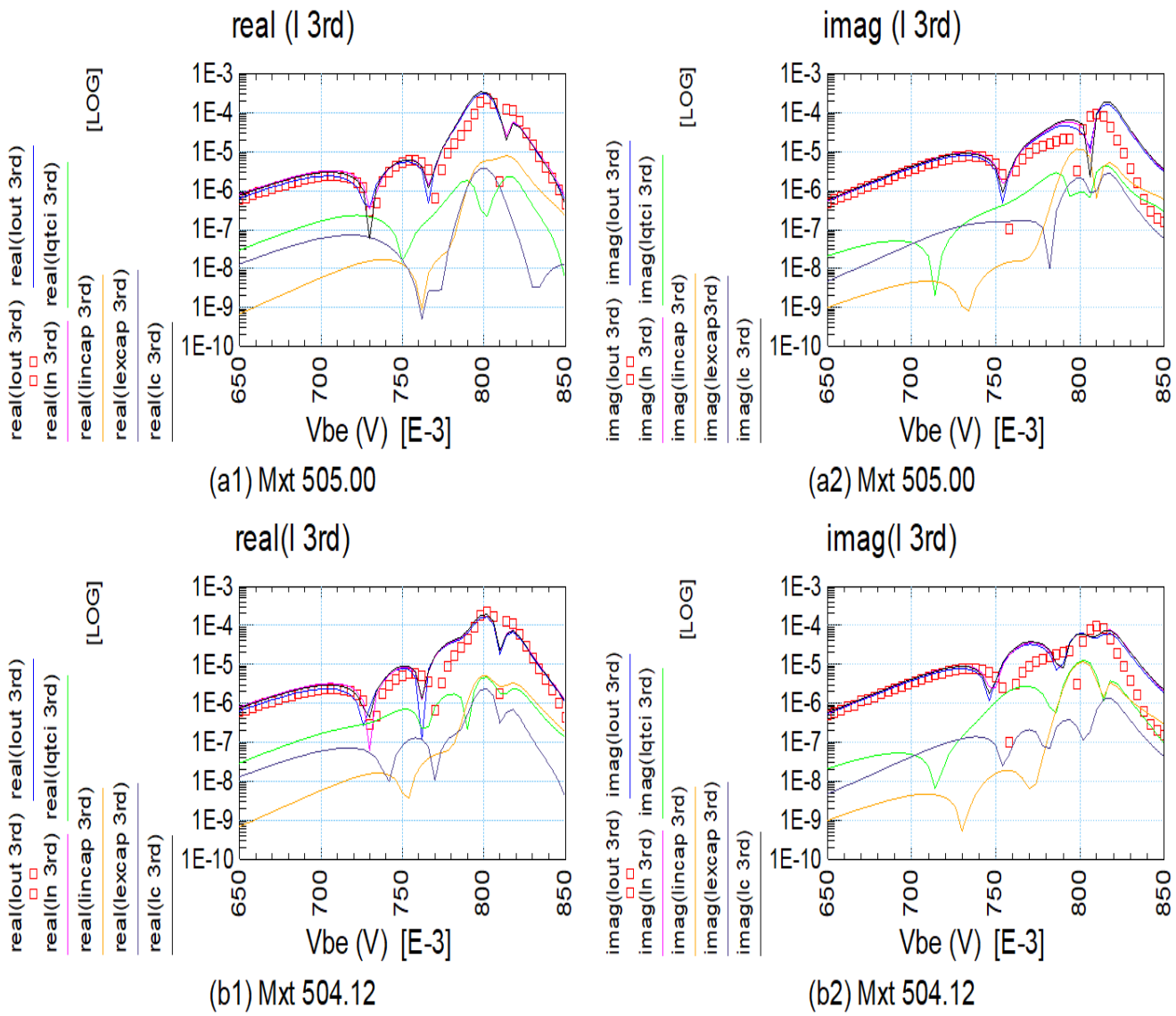

Figure 4.6: (a1) Real part of measured $i_{out,3rd}$ versus V_{BE} and real part of simulated $i_{out,3rd}$ and its component currents using Mextram 505.00 versus V_{BE}. (a2) imaginary part of measured $i_{out,3rd}$ versus V_{BE} and imaginary part of simulated $i_{out,3rd}$ and its component currents using Mextram 505.00 versus V_{BE}. (b1) Real part of measured $i_{out,3rd}$ versus V_{BE} and real part of simulated $i_{out,3rd}$ and its component currents using Mextram 504.12 versus V_{BE}. (b2) imaginary part of measured $i_{out,3rd}$ versus V_{BE} and imaginary part of simulated $i_{out,3rd}$ and its component currents using Mextram 504.12 versus V_{BE}.

4.4 Intrinsic CB Depletion Capacitance Effect on Third Order In

The intrinsic CB depletion capacitance affects third order I_n in two aspects. One is that the third order capacitance dynamic current possibly impacts on the third order I_n, and the other is that in Mextram I_n is calculated from the charge (V_{t_C}) of the intrinsic CB depletion capacitance in DC, V_{t_C} is the intrinsic capacitance charge normalized to the zero bias values, also the third order I_n may be affected by the intrinsic CB depletion capacitance.

In Mextram, I_n and Q_{tci}, charge of the intrinsic CB depletion capacitance, are given by:

$$I_n = \frac{I_s e^{\frac{V_{B_2E_1}}{V_T}} - I_s e^{\frac{V^*_{B_2C_2}}{V_T}}}{q_1^I(1 + 0.5(n0 + nB))}, \tag{4.6}$$

$$q_1^I = 1 + \frac{V_{t_E}}{V_{er}} + \frac{V_{t_C}}{V_{ef}}, \tag{4.7}$$

$$V_{t_C} = (1 - X_p)V_{C_V} + X_p V_{B_2C_1}, \tag{4.8}$$

$$V_{C_V} = \frac{V_{d_C ctc}}{1 - Pc}[1 - f_I(1 - V_{jC}/V_{d_C ctc})^{1-Pc}] + f_I b_{j_C}(V_{junc} - V_{jC}), \tag{4.9}$$

$$V_{jC} = V_{junc} - V_{ch}\ln(1 + \exp[(V_{junc} - V_{FC})/V_{ch}]), \tag{4.10}$$

$$Q_{tci} = XC_{jc}C_{jc}V_{tc}, \tag{4.11}$$

where I_s is a parameter of saturation current of main current, n_0 and n_B are electron densities at the edges of the neutral base region, V_{t_E} and V_{t_C} are charges of EB depletion capacitance and intrinsic CB depletion capacitance normalized to zero bias values, V_{er} and V_{ef} are parameters of reverse and forward early voltage. XC_{jc} and C_{jc} are parameters of the fraction of CB depletion capacitance under the emitter and the zero-bias CB depletion capacitance.

From Eq. (4.8) (4.9) (4.10), giving different V_{junc} and V_{ch} options, the intrinsic CB depletion capacitance will be changed, q_1^I and Q_{tci} will also be changed from Eq. (4.7) (4.11). If $q1I$ is changed, from the Mextram I_n equation, the third order I_n might be changed. The third order I_n can be affected by the intrinsic CB depletion capacitance through Early effect

by q_1^I. If Q_{tci} is changed, the dynamic charging current will be changed, and from the Mextram equivalent circuit Figure 4.5, the third order I_n can be impacted by this dynamic charging current. That means the third order I_n can be impacted by the intrinsic CB depletion capacitance through the dynamic charging current by Q_{tci}. It is essential to figure out if the intrinsic CB depletion capacitance affects the third order I_n through q_1^I or Q_{tci}.

The different intrinsic CB depletion capacitance in Mextram 505 and Mextram 504 give different q_1^I and different Q_{tci}, we can modify Verilog-a code to have 4 combinations (2x2) OIP3, OIP3 with 505 q_1^I and 505 Q_{tci}, OIP3 with 504 q_1^I and 504 Q_{tci}, OIP3 with 505 q_1^I and 504 Q_{tci}, OIP3 with 504 q_1^I and 505 Q_{tci}. If using the same q_1^I but different Q_{tci} can give different OIP3 and different $I_{n,3rd}$, the conclusion is that the intrinsic CB depletion capacitance affects OIP3 and $I_{n,3rd}$ through third order dynamic charging current. If using the same Q_{tci} but different q_1^I gives different OIP3 and different $I_{n,3rd}$, the conclusion is that the intrinsic CB depletion capacitance affects OIP3 and $I_{n,3rd}$ through Early effect, and the parameter V_{ef} is very important to OIP3.

Figure 4.7 (a) shows measured OIP3-V_{BE} by symbols, simulated OIP3-V_{BE} with 505 q_1^I and 505 Q_{tci} in blue and simulated OIP3-V_{BE} with 504 q_1^I and 505 Q_{tci} in black. Figure 4.7 (b) shows simulated mag($I_{n,3rd}$)-V_{BE} with 505 q_1^I and 505 Q_{tci} in blue and simulated mag($I_{n,3rd}$)-V_{BE} with 504 q_1^I and 505 Q_{tci} in black. Figure 4.7 (a) (b) compare OIP3-V_{BE} and mag($I_{n,3rd}$)-V_{BE} simulated using the same Q_{tci}, but with different q_1^I. Neither OIP3 nor mag($I_{n,3rd}$) are affected when we intentionally used the different q_1^I corresponding to the same Q_{tci}. This implies the intrinsic CB depletion capacitance can not impact on IP3 and $I_{n,3rd}$ by q_1^I. Furthermore, changing the parameter V_{ef} in OIP3 simulations in Mextram 504 and in Mextram 505, both OIP3 simulations are not changed, hence those simulations are not shown. This also proves that q_1^I has no effect on OIP3.

Figure 4.8 (a) shows measured OIP3-V_{BE} by symbols, simulated OIP3-V_{BE} with 504 q_1^I and 505 Q_{tci} in blue and simulated OIP3-V_{BE} with 504 q_1^I and 504 Q_{tci} in black. Figure 4.7 (b) shows simulated mag($I_{n,3rd}$)-V_{BE} with 504 q_1^I and 505 Q_{tci} in blue and simulated

mag($I_{n,3rd}$)-V_{BE} with 504 q_1^I and 504 Q_{tci} in black. Figure 4.8 (a) (b) compare OIP3-V_{BE} and mag($I_{n,3rd}$)-V_{BE} simulated using the same q_1^I, but with different Q_{tci}. OIP3 and mag($I_{n,3rd}$) are affected when we intentionally used the different Q_{tci} corresponding to the same q_1^I. This implies that the dynamic current change is the main mechanism by which intrinsic CB depletion capacitance affect IP3.

Now it is clear that the intrinsic CB depletion capacitance does not impact the $I_{n,3rd}$ and OIP3 through Early effect, but it affects the $I_{n,3rd}$ and OIP3 through capacitance dynamic current and circuit action.

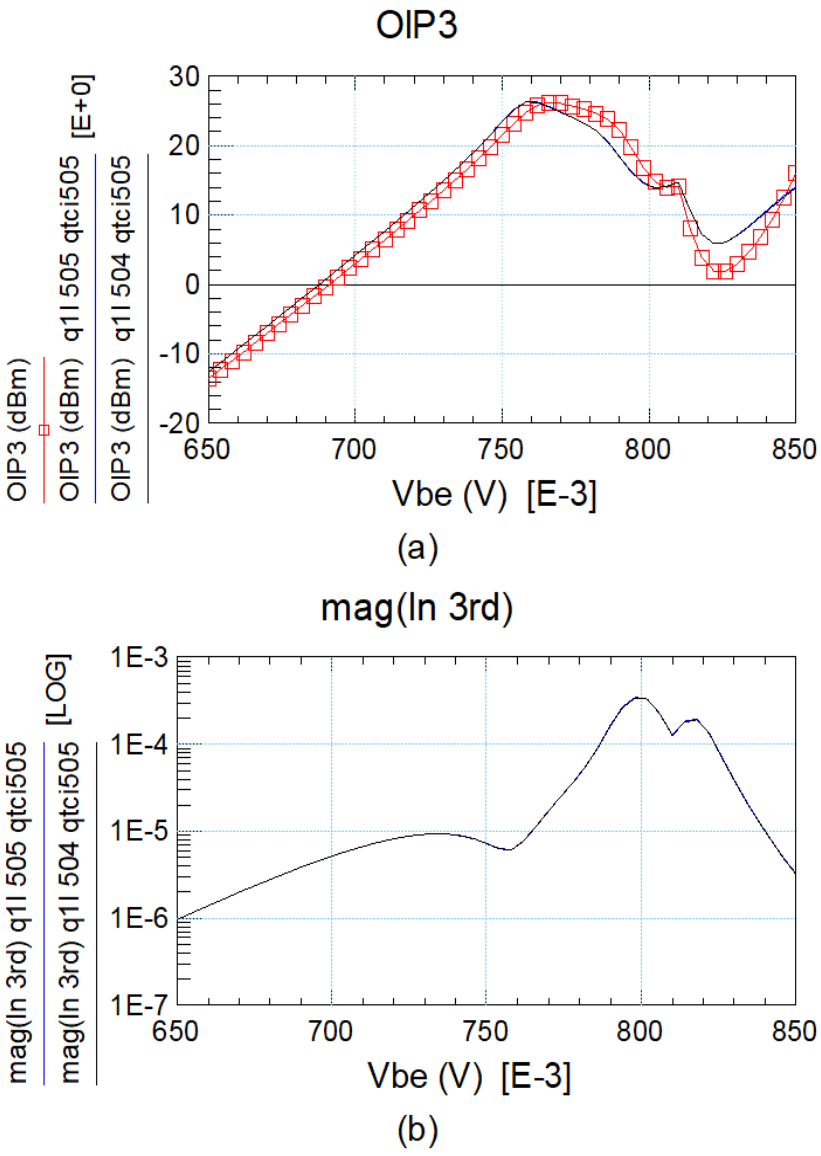

Figure 4.7: (a) Measured OIP3 and simulated OIP3 with different q_1^I but the same Q_{tci} versus V_{BE}. (b) Simulated mag($i_{n,3rd}$) with different q_1^I but the same Q_{tci} versus V_{BE}.

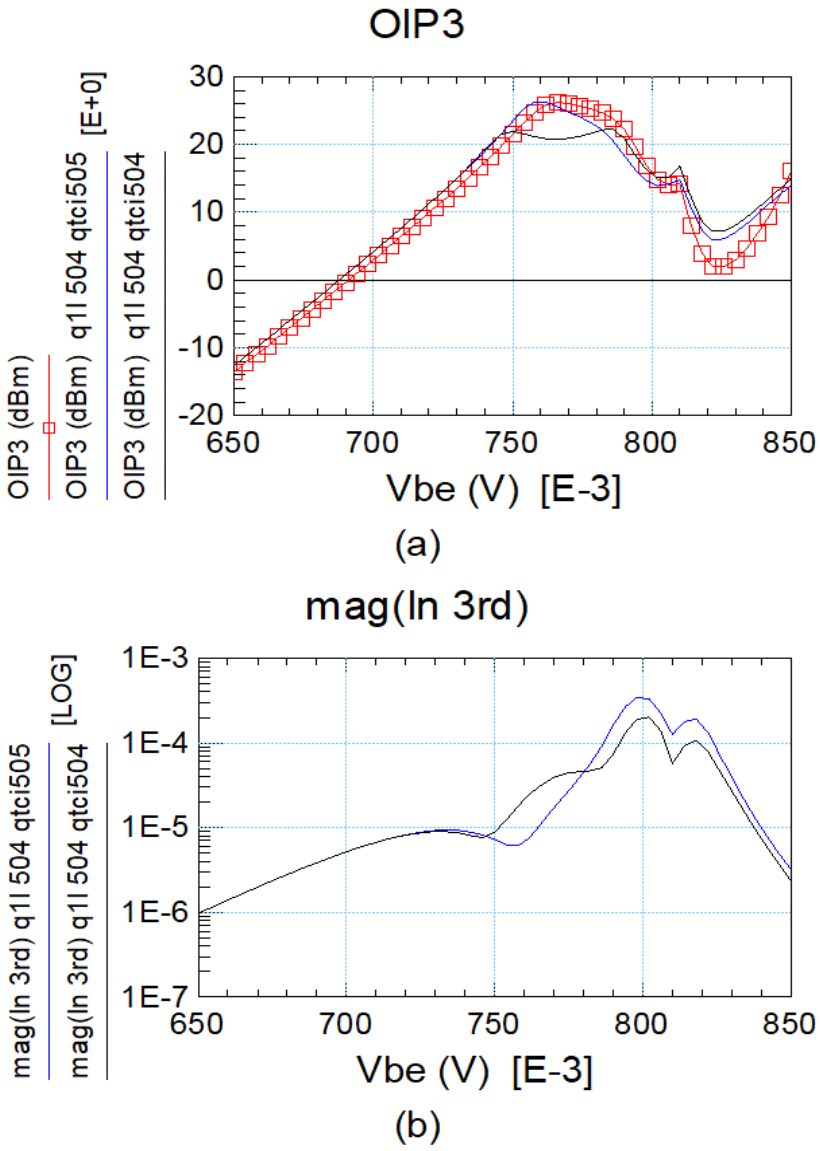

Figure 4.8: (a) Measured OIP3 and simulated OIP3 with different Q_{tci} but the same q_1^I versus V_{BE}. (b) Simulated mag($i_{n,3rd}$) with different Q_{tci} but the same q_1^I versus V_{BE}.

Parameter XC_{jc}, C_{jc}	Capacitance Q_{tci}, Q_{tcx}
$C_{jc} \neq 0$, $XC_{jc} = 0.7$	Q_{tci}, Q_{tcx}
$C_{jc} \neq 0$, $XC_{jc} = 1$	Q_{tci}, $Q_{tcx} = 0$
$C_{jc} \neq 0$, $XC_{jc} = 0$	$Q_{tci} = 0$, Q_{tcx}
$C_{jc} = 0$	$Q_{tci} = 0$, $Q_{tcx} = 0$

Table 4.1: Capacitances and their related parameters.

4.5 Intrinsic and Extrinsic CB Depletion Capacitance Effect on OIP3

In Mextram, CB depletion capacitance has intrinsic part and extrinsic part. The intrinsic CB depletion capacitance has a big effect on OIP3, the extrinsic CB depletion capacitance also should be taken into account. Q_{tcx} and Q_{tci} are charges of the intrinsic and the extrinsic CB depletion capacitance.

To know how dose Q_{tci} and Q_{tcx} affect IP3, we can change the CB capacitance parameters XC_{jc} and C_{jc}. The intrinsic CB capacitance charge Q_{tci} can be disabled by setting the parameter $XC_{jc} = 0$, so that all capacitance is the extrinsic capacitance. The extrinsic CB capacitance charge Q_{tcx} can be disabled by setting the parameter $XC_{jc} = 1$, so that all capacitance is the intrinsic capacitance. Both the intrinsic and the extrinsic capacitance can be disabled by setting the parameter $C_{jc} = 0$.

Table 4.1 shows capacitance parameters with different values and their related capacitances, $XC_{jc} = 0.7$ is the value extracted from measurement. These parameter values are used in OIP3 simulations in figure 4.9 (a) (b) and figure 4.10 (a) (b) (c).

Figure 4.9 (a) shows measurement of OIP3-V_{BE} by symbols and simulations of OIP3-V_{BE} using Mextram 505.00, simulated OIP3-V_{BE} with $XC_{jc} = 0.7$ in blue, simulated OIP3-V_{BE} with $XC_{jc} = 0$ in pink, simulated OIP3-V_{BE} with $XC_{jc} = 1$ in black, simulated OIP3-V_{BE} with $C_{jc} = 0$ in green. Figure 4.9 (b) shows measurement of OIP3-V_{BE} by symbols and simulations of OIP3-V_{BE} using Mextram 504.12, simulated OIP3-V_{BE} with $XC_{jc} = 0.7$ in blue, simulated OIP3-V_{BE} with $XC_{jc} = 0$ in pink, simulated OIP3-V_{BE} with $XC_{jc} = 1$ in black, simulated OIP3-V_{BE} with $C_{jc} = 0$ in green. Figure 4.9 (a) (b) compare OIP3-V_{BE} respectively in Mextram 504.12 and in Mextram 505.00 with the parameters $XC_{jc} = 0$,

$XC_{jc} = 1$, $XC_{jc} = 0.7$ and $C_{jc} = 0$. The OIP3 is affected when the parameters have different values. This indicates that both the intrinsic and the extrinsic capacitance can affect OIP3 and the ratio XC_{jc} of intrinsic and extrinsic capacitance also impacts OIP3.

Figure 4.10 (a) shows measured OIP3-V_{BE} by symbols and simulated OIP3-V_{BE} using Mextram 505.00 in blue and 504.12 in black for $XC_{jc} = 0.7$. Figure 4.10 (b) shows measured OIP3-V_{BE} by symbols and simulated OIP3-V_{BE} using Mextram 505.00 in blue and 504.12 in black for $XC_{jc} = 0$. Figure 4.10 (c) shows measured OIP3-V_{BE} by symbols and simulated OIP3-V_{BE} using Mextram 505.00 in blue and 504.12 in black for $C_{jc} = 0$.

Comparing Figure 4.10 (a) with Figure 4.10 (b), OIP3 simulations in Mextram 504.12 and 505.00 become the same when the intrinsic CB depletion capacitance is disabled, since Mextram 504.12 and 505.00 have different intrinsic CB depletion capacitances but the same extrinsic CB depletion capacitances. This implies that Q_{tci} difference makes OIP3 difference, but q_1^I difference does not cause OIP3 difference. By comparing Figure 4.10 (b) with Figure 4.10 (c), OIP3 are affected when the extrinsic CB depletion capacitance is disabled. Decreasing the extrinsic capacitance improves the peak OIP3, which is significant. This suggests the importance of minimizing extrinsic CB depletion capacitance for improved OIP3.

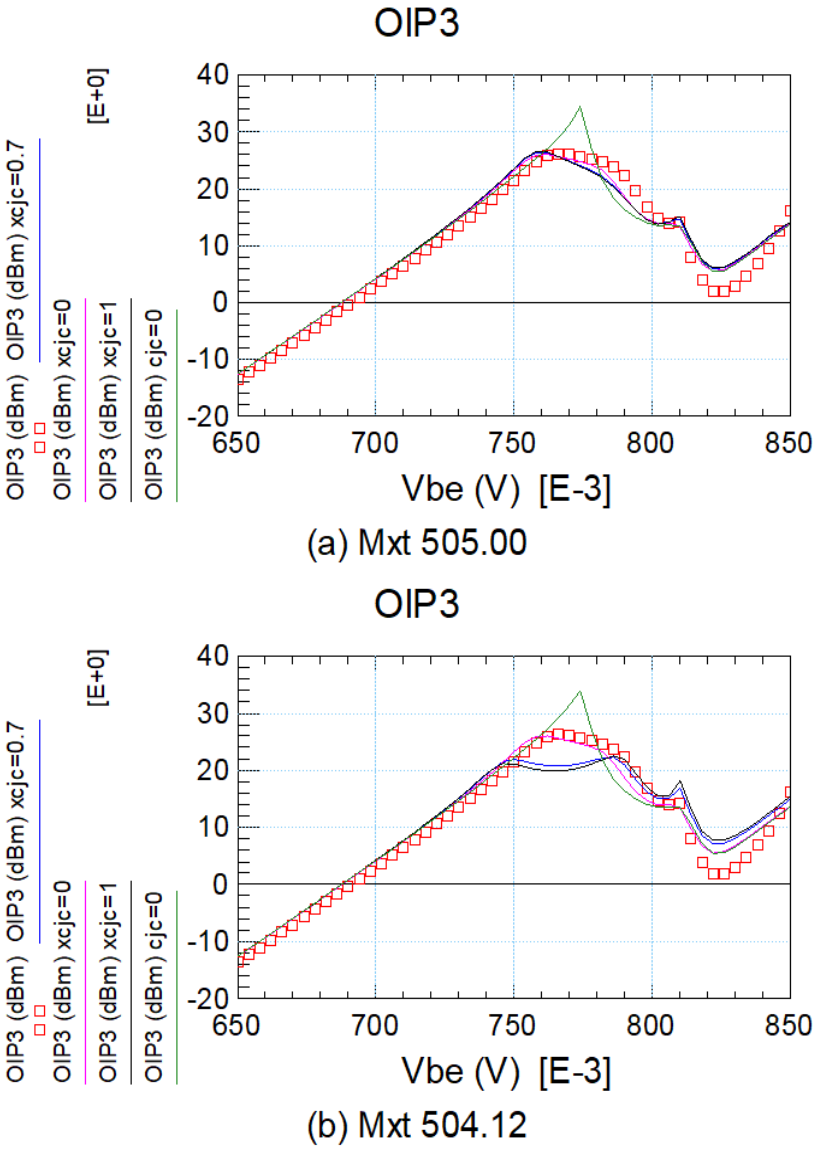

Figure 4.9: (a) Measured OIP3 and simulated OIP3 using Mextram 505.00 with different XC_{jc} and different C_{jc} versus V_{BE}. (b) Measured OIP3 and simulated OIP3 using Mextram 504.12 with different XC_{jc} and different C_{jc} versus V_{BE}.

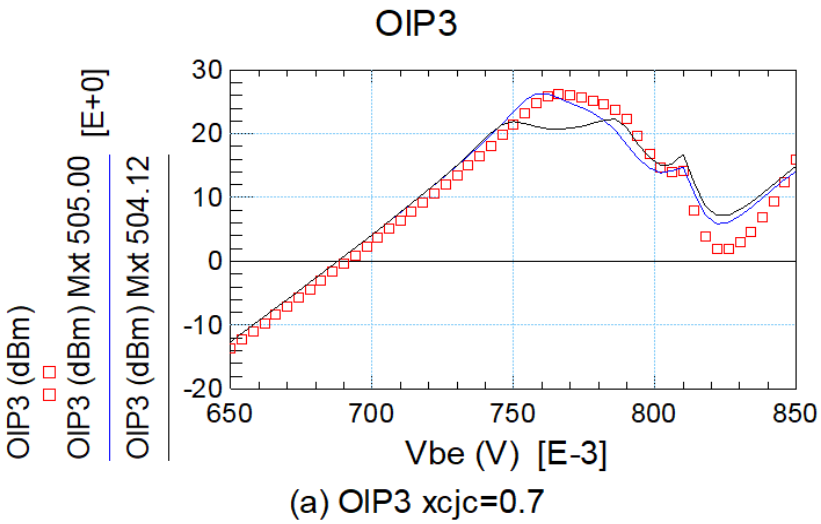

(a) OIP3 xcjc=0.7

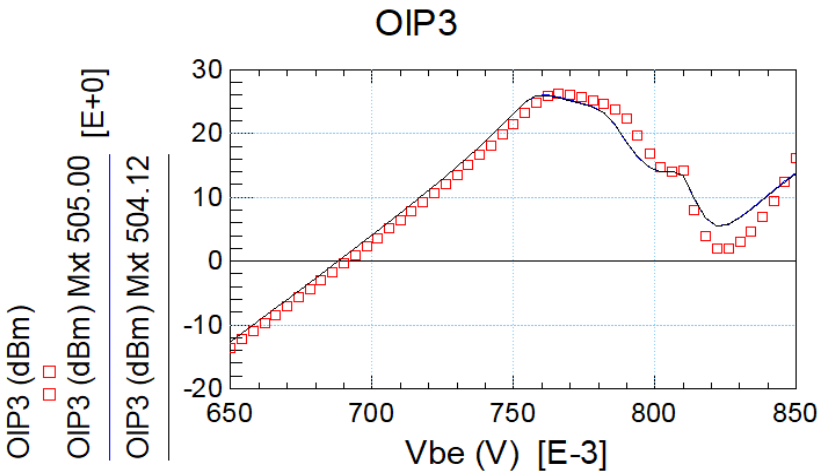

(b) OIP3 xcjc=0

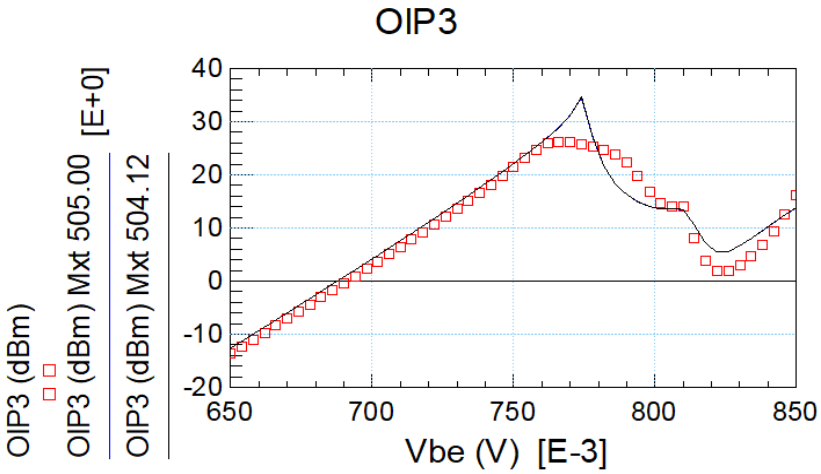

(c) OIP3 cjc=0

Figure 4.10: (a) Measured OIP3 and simulated OIP3 using Mextram 504.12 and 505.00 with $XC_{jc} = 0.7$ versus V_{BE}. (b) Measured OIP3 and simulated OIP3 using Mextram 504.12 and 505.00 with $XC_{jc} = 0$ versus V_{BE}. (c) Measured OIP3 and simulated OIP3 using Mextram 504.12 and 505.00 with $C_{jc} = 0$ versus V_{BE}.

4.6 Intrinsic and Extrinsic CB Depletion Capacitance Effect on Third Order In

It is known that both the intrinsic and the extrinsic CB depletion capacitance affect OIP3 and the intrinsic CB depletion capacitance affects the third order I_n through dynamic charging current to change OIP3. Now it is necessary to see how does the intrinsic and the extrinsic CB depletion capacitance impact on the third order I_n.

To know how does the two capacitances affect the third order I_n to change OIP3, we can change the CB depletion capacitance parameters XC_{jc} and C_{jc}, the same way used in the last section. Setting parameters $XC_{jc} = 0.7$, $XC_{jc} = 0$ and $C_{jc} = 0$ respectively, three groups of third order I_n simulations can be obtained, which are $I_{n,3rd}$ simulated with both Q_{tci} and Q_{tcx}, $I_{n,3rd}$ simulated with only Q_{tcx}, and $I_{n,3rd}$ simulated with no CB depletion capacitance.

Figure 4.11 (a1) (a2) (a3) show simulated real part, imaginary part and magnitude of $i_{n,3rd}$ using Mextram 504.12 and 505.00 with Q_{tci} and Q_{tcx}. Figure 4.11 (b1) (b2) (b3) show simulated real part, imaginary part and magnitude of $i_{n,3rd}$ using Mextram 504.12 and Mextram 505.00 with only Q_{tcx}. Figure 4.11 (c1) (c2) (c3) show simulated real part, imaginary part and magnitude of $i_{n,3rd}$ using Mextram 504.12 and 505.00 with no CB depletion capacitance. Comparing Figure 4.11 (a1) (a2) (a3) with Figure 4.11 (b1) (b2) (b3), the real part, imaginary part and magnitude of $i_{n,3rd}$ become the same when Q_{tci} is disabled. This implies the intrinsic CB depletion capacitance affect the third order I_n to change OIP3. Comparing Figure 4.11 (b1) (b2) (b3) with Figure 4.11 (c1) (c2) (c3), the real part, imaginary part and magnitude of $i_{n,3rd}$ are affected when Q_{tcx} is disabled. This implies the extrinsic CB depletion capacitance also affects the third order I_n. That means both the intrinsic and the extrinsic CB depletion capacitance impact on the third order I_n.

It is known OIP3 is mainly determined by the third order I_n not the first order I_n, but CB depletion capacitance effect on the first order I_n should be take into account. To know how does the CB depletion capacitance affect the first order I_n, the first order I_n is simulated in the same way as the third order I_n.

Figure 4.12 (a1) (a2) (a3) show simulated real part, imaginary part and magnitude of $i_{n,1st}$ using Mextram 504.12 and 505.00 with Q_{tci} and Q_{tcx}. Figure 4.12 (b1) (b2) (b3) show simulated real part, imaginary part and magnitude of $i_{n,1st}$ using Mextram 504.12 and 505.00 with only Q_{tcx}. Figure 4.12 (c1) (c2) (c3) show simulated real part, imaginary part and magnitude of $i_{n,1st}$ using Mextram 504.12 and 505.00 with no CB depletion capacitance. Figure 4.12 (a1) (a2) (a3) compare the real part, imaginary part and magnitude of $i_{n,1st}$ between Mextram 504.12 with 505.00. The real part, imaginary part and magnitude of the $i_{n,1st}$ have a little difference. This implies the intrinsic CB depletion capacitance has a mild effect on the first order I_n. Comparing Figure 4.12 (b1) (b2) (b3) with Figure 4.12 (c1) (c2) (c3), the real part, imaginary part and magnitude of $i_{n,1st}$ have a little difference when Q_{tcx} is disabled. This implies the extrinsic CB depletion capacitance also has a slight effect on the first order I_n. That means both the intrinsic and the extrinsic CB depletion capacitance impact on the third order I_n lightly.

Both the intrinsic and the extrinsic CB depletion capacitance affect the third order main current and the first order main current. The two capacitance mainly impact on the third order main current to change OIP3, since they have a much bigger effect on the third order main current compared to the first order main current.

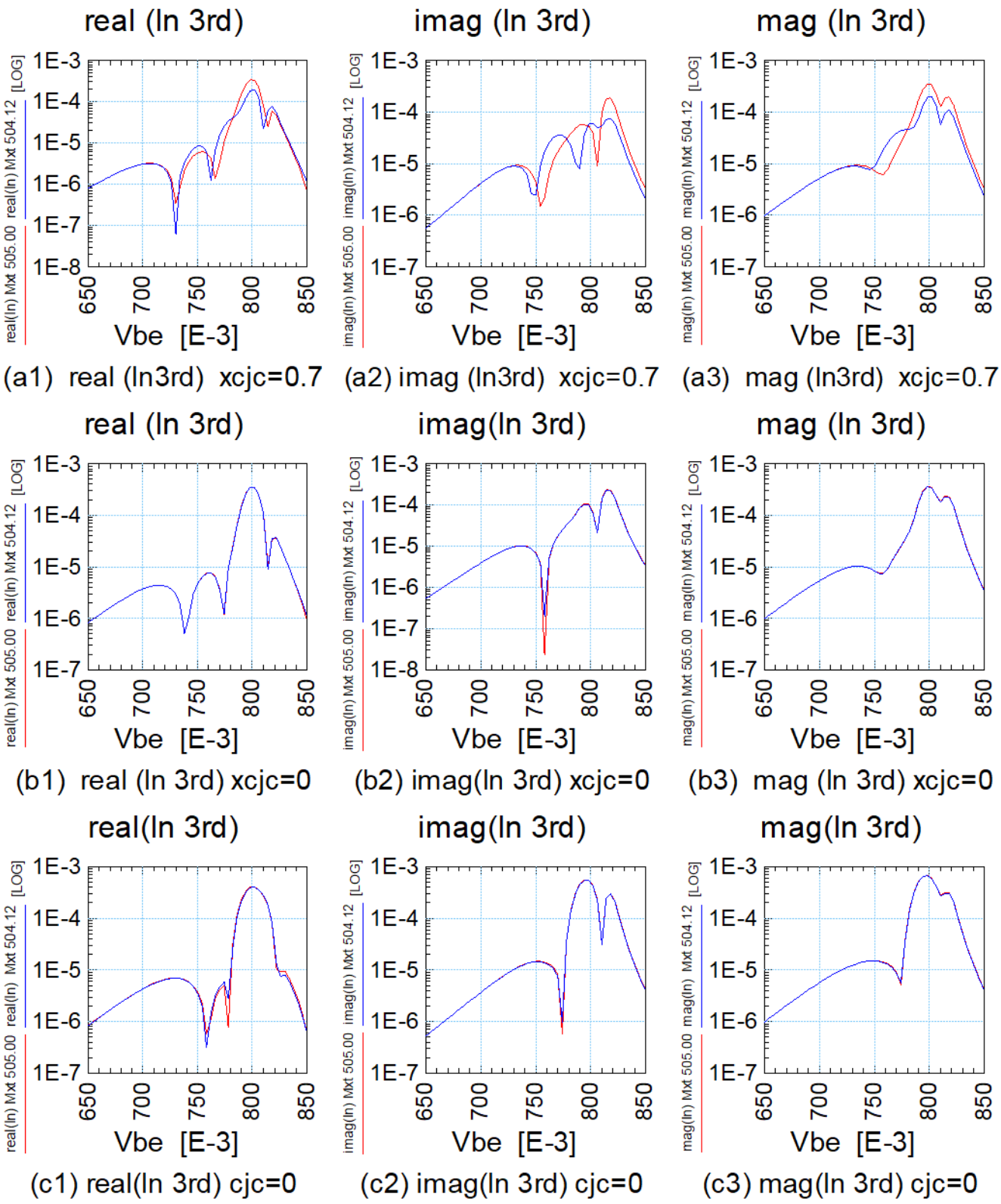

Figure 4.11: (a1) (a2) (a3) Simulated real part, imaginary part and magnitude of $i_{n,3rd}$ using Mextram 504.12 and 505.00 for $XC_{jc} = 0.7$. (b1) (b2) (b3) Simulated real part, imaginary part and magnitude of $i_{n,3rd}$ using Mextram 504.12 and 505.00 for $XC_{jc} = 0$. (c1) (c2) (c3) Simulated real part, imaginary part and magnitude of $i_{n,3rd}$ using Mextram 504.12 and 505.00 for $C_{jc} = 0$.

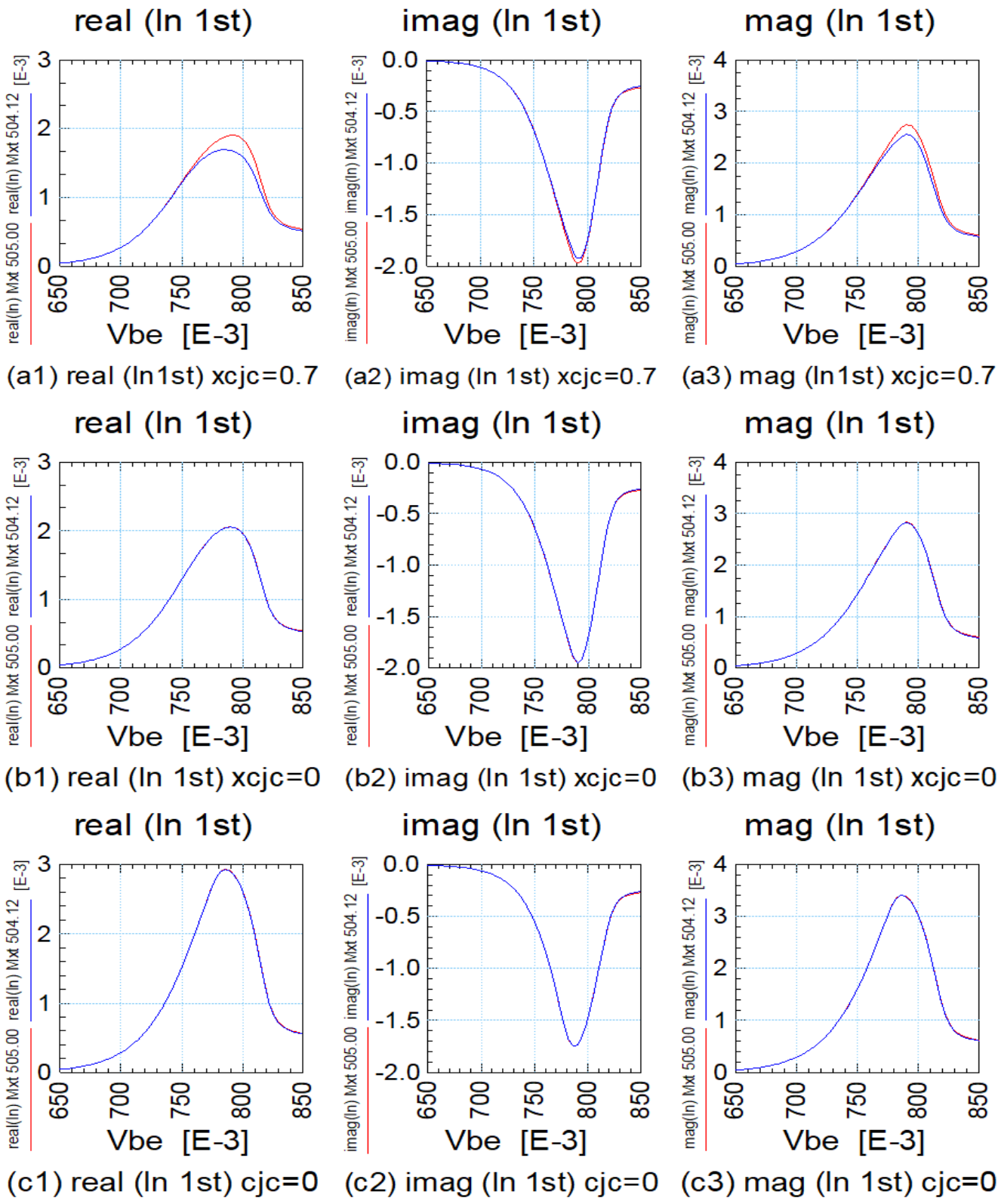

Figure 4.12: (a1) (a2) (a3) Simulated real part, imaginary part and magnitude of $i_{n,1st}$ using Mextram 504.12 and 505.00 for $XC_{jc} = 0.7$. (b1) (b2) (b3) Simulated real part, imaginary part and magnitude of $i_{n,1st}$ using Mextram 504.12 and 505.00 for $XC_{jc} = 0$. (c1) (c2) (c3) Simulated real part, imaginary part and magnitude of $i_{n,1st}$ using Mextram 504.12 and 505.00 for $C_{jc} = 0$.

4.7 Summary

In this chapter, the linearity characteristics of the CE configuration were dealt with in detail. Mextram 505.00 provides a much better OIP3 modeling than Mextram 504.12 by modifying the intrinsic CB depletion capacitance. Comparing the first order output current with the third order output current, OIP3 is mainly determined by the third order output current. However, in the third order output current, the third order main current is dominant, so the OIP3 mainly depends on the third order main current. Both the intrinsic and the extrinsic CB depletion capacitance affect main currents to change OIP3. The two capacitance mainly impact on the third order main current to affect OIP3, since they have a slight effect on the first order main current. The intrinsic CB depletion capacitance impacts on the third order main current through dynamic charging current to make OIP3 difference. The extrinsic CB depletion capacitance has a big effect on OIP3, that decreasing the extrinsic CB depletion capacitance can improve the peak OIP3.

Bibliography

[1] J.D. Cressler, "SiGe HBT Technology: A New Contender for Si-based RF and Microwave Circuit Applications," *IEEE Transactions on Microwave Theory and Techniques*, vol.46, pp.572-589, May 1998.

[2] Z. Xu, "Physics, Modeling and Design Implications of RF Correlation Noise in SiGe HBTs," *Auburn University*, 2013.

[3] J. D. Cressler and G. F. Niu, "Silicon-Germanium Heterojunction Junction Bipolar Transistors" Artech House, 2003.

[4] G. Niu, R. V. D. Toorn, J. C. J. Paasschens, W.J. Kloosterman, , *The Mextram Bipolar Transistor Model Definition*, Auburn University, 2017.

[5] S. Seth, "Understanding Distortion in Silicon-Germanium Transistor, and Its Application to RF Circuits," *Georgia Institute of Technology*, 2009.

[6] J. C. J. Paasschens, W.J. Kloosterman, R. V. D. Toorn, *Model Derivation of Mextram 504: The Physics behind the Model*, Koninklijke Philips Electronics, 2004.